Investigating the Long-Range, Near-Side Two-Particle Correlation Ridge Using ATLAS Recorded $\sqrt{s} = 7$ TeV Proton-Proton Collisions

Adam Stewart

Supervised by Dr. William Murray

School of Physics & Astronomy

University of Southampton
Southampton
SO17 1BJ
UK

adam.stewart@cern.ch

May 2011

Acknowledgements

I would like to thank my supervisor, Dr. Bill Murray, for his help and guidance during the progression of all aspects of the project. Additionally I express my thanks to Dr. Jan Strube for his technical help and supply of data. I would also like to express my gratitude to various people from ATLAS working groups, including: the Jet and Missing Et group, for their advice and help in jet analysis; the Standard Model working group, for support with the data formatting and obtaining access to the trigger information; and the two-particle correlations group, especially those based at the University of Glasgow, for their thoughts and suggestions during the project. Finally, I thank my father Paul Stewart and brother Graeme Stewart; along with James Ryan and Sam Lawrence for all their very helpful comments and suggestions during the writing of this document.

Abstract

Results are presented on the attempt to observe a long-range, near-side ridge in the two-particle angular correlation function ($R(\Delta\eta, \Delta\phi)$), analogous to the unexpected observation presented by the CMS collaboration in September, 2010. A result which hinted at the presence of a hot, dense medium in proton-proton collisions. The possibility of a prosaic interpretation of the ridge, specifically that of a colour string effect, is investigated. This was performed by analysing 2010 proton-proton collision data with $\sqrt{s} = 7$ TeV, recorded by the ATLAS detector at the LHC. Descriptions are provided of the analysis, data handling, quality control and trigger selection, all of which were developed specifically for the investigation. The results, entirely a product of this study, exhibit intriguing features when high multiplicity events are analysed along with requesting a high sum of the total energy of all the jets - at approximately 1.3 TeV or greater. However, overall the results are inconclusive, thus possibly implying at a quark gluon plasma being produced in proton-proton collisions.

Contents

List of Figures

List of Tables

Chapter 1

Introduction

1.1 CMS Observation

In September 2010, the CMS Collaboration presented to the scientific community one of the most intriguing observations to emerge from the first data running period of the Large Hadron Collider (LHC) [1]. It detailed the appearance of a pronounced structure, named *the ridge*, when studying two-particle angular correlations of proton-proton (pp) collisions with a centre-of-mass energy ($\sqrt{s}$) of 7 TeV. Interestingly, this effect was not expected as it had not previously been observed in any Monte Carlo simulations. The result was obtained by utilising the two dimensional $\Delta\eta$-$\Delta\phi$ correlation functions, where firstly, $\Delta\eta$ is defined as the difference in pseudorapidity, η, between the two charged particles ($\eta = -\ln(\tan(\theta/2))$, θ is defined as the polar angle with respect to the beam axis). Secondly, $\Delta\phi$ is the difference between the two charged particles azimuthal angle ϕ, which is measured around the beam axis.

Figure 1.1 shows the main, 2-D two-particle correlation plots from the CMS study, with (a) and (b) showing the analysis performed upon *minimum bias* events, in the transverse momentum range of $p_T > 0.1$ GeV/c and then a specific range of 1 GeV/c $< p_T <$ 3 GeV/c respectively. Plots (c) and (d) on the other hand present the same, but in this case high multiplicity events have been analysed instead of minimum bias, specifically events which had a multiplicity, N, > 110. While plots (a, b & c) showed nothing that deviated from theoretical models, plot (d) clearly displayed an unexpected ridge structure in the long-range, near-side region. In particular it was discovered to arise in the region of $2.0 < |\Delta\eta| < 4.8$ and $\Delta\phi \approx 0$, and only appeared in these high multiplicity events, in the aforementioned intermediate 1 GeV/c - 3 GeV/c p_T range.

This type of correlation had not been observed in pp collisions before, and therefore no physical origin was described by CMS along with the observation. Yet, what made the result very interesting was that it was reminiscent of such a correlation observed in data collected by experiments at the Relativistic Heavy Ion Collider (RHIC); whose main aim is to create and study the state of matter known as *Quark Gluon Plasma* (QGP): a (locally) thermally equilibrated

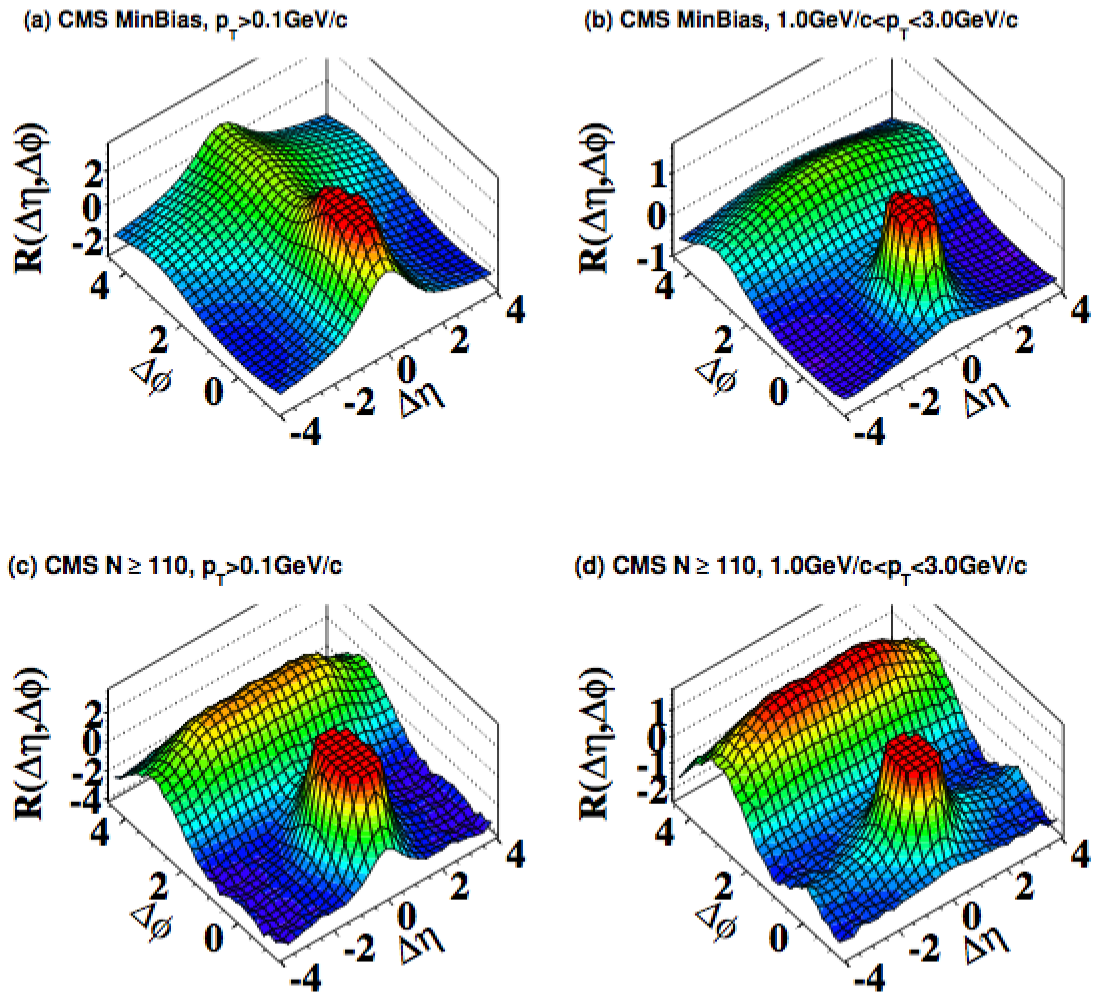

Figure 1.1: *The above are the results presented by the CMS collaboration. Plots (a) and (b) are results from the minimum bias in the p_T ranges stated by the plots. Histograms (c) and (d) show the same p_T ranges but now are requesting high multiplicity events, where the ridge was seen to emerge in (d). Plots from referece [1].*

state of matter in which quarks and gluons are deconfined from hadrons [2].

1.2 Two-Particle Correlations Studies

1.2.1 Features of the 2-D Correlation Plot

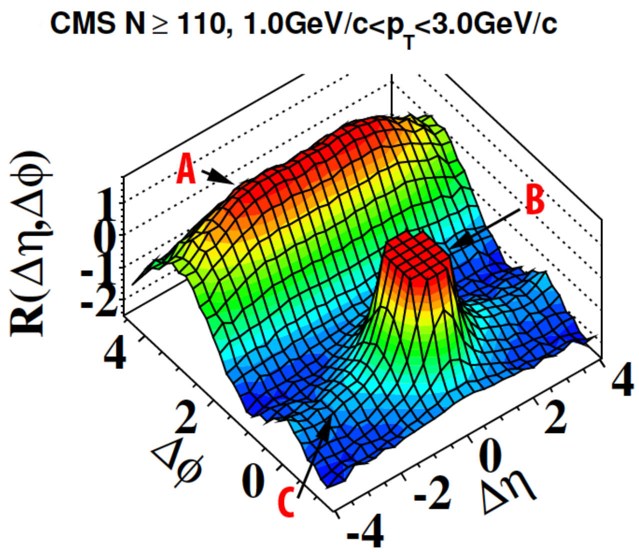

Figure 1.2: *A closer look at the 2-D two-particle correlation plot from CMS which displays the ridge. Feature A is known as the away side ridge, feature B is the near side jet peak and feature C is the newly discovered ridge feature. A more detailed description of the features can be found in the text below.*

Figure 1.2 displays a magnified version of the CMS ridge plot as seen in Figure 1.1(d). Apart from the newly discovered ridge there are two other main features, both of which can be easily explained. The feature labelled **A**, at $\Delta\phi \approx \pi$ and extended in $\Delta\eta$ is named the *away side ridge*; it is explained by the balancing of the transverse momentum p_T in the near region, or in other words, back-to-back jets. So a particle belonging to one jet will have a correlation angle of $\Delta\phi \approx \pi$, with a particle belonging to the opposite momentum balancing jet, though the correlation in $\Delta\eta$ can be any value in the valid range of -5 to 5 (this is simply due to the detector coverage, however the plots presented are cut at $|\Delta\eta| < 4$, reasons as to why are discussed later in Section 4.2.5). The main peak centred at $(\Delta\eta, \Delta\phi) = (0, 0)$, labelled **B**, is simply the correlations between particles in the same jet, thus approximately zero would be expected in both cases. This leaves the suspected new physics feature of the ridge, labelled **C**.

1.2.2 Reasons for Study & Previous Investigations

Studying two-particle correlations provides a very useful tool with which to investigate the underlying mechanisms of particle production. Models which describe multi-particle production such as the string model, where particle production is described by the fragmentation of *colour strings* [3], or the cluster model, a process where intermediate objects are created called clusters, which then decay into the particles which are observed [4], are known to be incomplete. Investigating two-particle correlations can offer valuable dynamic information that could be integrated into such models in order to improve them; and to gain a more general understanding of the processes [5].

As mentioned in the preceding section, experiments at RHIC such as STAR [6] (Solenoidal Tracker at RHIC), have previously performed two-particle angular correlation studies on heavy ion collisions, in particular Gold-Gold (Au-Au) collisions at $\sqrt{s_{NN}} = 200$ GeV. Figure 1.3 shows a 2-D correlation result, where the events are central[1] Au-Au collisions. Here a clear ridge is visible, and with its extent in $\Delta\eta$, it was suggested that the structure in the correlation was formed early on in the fireball that proceeded the initial central collision; a fireball which went on to form a QGP state of matter (a detailed look at the evolution of QGP in heavy ion collisions can be found in Section 2.1). This led some to hypothesise that the ridge observed by CMS, was a hint of a QGP-like substance being created in pp collisions for the first time; which would not be expected at such a low parton density.

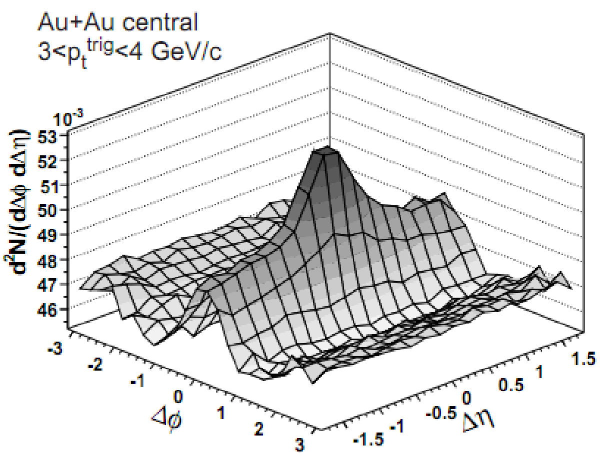

Figure 1.3: *The ridge, as observed at RHIC in Au-Au collisions by the STAR experiment. The process that created this feature could be what produced the CMS ridge in the high energy pp collisions. [7].*

[1]Centrality is a term used to define the impact parameter in heavy ion collisions. Counter intuitively, a low centrality means the collisions occur with a finite impact parameter, i.e. a quite head on collision. Therefore high centrality refers to those collisions which have quite a large impact parameter and could be described as grazing collisions.

1.3 Aim & Outline

The emergence of a QGP-like medium is not the only theory put forward to explain the ridge. One fairly popular alternative source is that it originates from colour string fragmentation [8]. In a simplistic explanation; an outgoing parton as a result of the interaction, would need to colour neutralise with the remnant proton travelling in the direction of the beam pipe. This would cause a string to manifest between the two, with its eventual fragmentation giving rise to extra emissions. When analysing two-particle correlations, these extra emissions could potentially form a ridge; analogous to that observed by CMS.

The aim of this investigation was to search for a ridge in the two-particle correlation function that arises from the string model mentioned above. To achieve this, jet events from pp collisions at $\sqrt{s}$ = 7 TeV, recorded by the ATLAS detector, were analysed. This study had the potential to add evidence on either side of the QGP argument - if a ridge was seen then it would cast doubt on whether what was observed was really caused by the presence of a QGP-like state of matter; on the other hand, if no ridge correlation was found, then the case for the aforementioned argument of QGP production could be strengthened.

The general method of the analysis was very analogous to that which CMS performed, while adding various cuts and selections based upon colour strings being the potential source of the ridge (refer to Section 2.2 for detailed description of the cuts). This is currently just a component of the work being performed at ATLAS into investigating the ridge. For example, work elsewhere is attempting to completely replicate CMS's study; it is interesting to note that as of writing, this group is yet to observe any evidence of a ridge structure [5]. However, problems arise with the ATLAS dataset not being suitable for this type of analysis, due to the lack of a sufficient high multiplicity trigger (which CMS developed and dedicated bandwidth to at the hint of this signal). This has led to an attempt to develop a high multiplicity trigger for future running. As an aside of this investigation, heavy ion data consisting of Lead-Lead (Pb-Pb) collisions at $\sqrt{s_{NN}}$ = 2.76 TeV, recorded by the ATLAS detector during the late 2010 LHC heavy ion run, has also been briefly analysed.

More detailed discussion of the possible interpretations of the ridge, along with its comparable nature to results seen in heavy ion collisions, plus the theory of the investigation, are discussed in Chapter 2. The general method used to calculate the two-particle correlation function is then outlined in Chapter 3. Hereafter the investigation has two distinct halves: Chapter 4 details the data used and the results gained from the early half of the analysis, including results from the heavy ion data. Chapter 5 then presents the modifications made to the method ensuing the early results, and displays and discusses the most current results. This report ends with Chapter 6 which draws conclusions from all the work performed during the investigation.

Chapter 2

Theory

2.1 Quark Gluon Plasma

2.1.1 Quark Confinement & The Plasma

One feature of Quantum Chromodynamics (QCD), for reasons that are not yet fully understood, is that quarks are confined to colourless packages of either two quarks or three quarks, i.e. Mesons and Baryons respectively [9]. As two quarks are pulled apart, strings of colour charge form between them until it becomes energetically favourable to create new quarks, which sequentially connect to the original quarks to form hadrons. For this reason a quark has never been observed alone. Figure 2.1 gives an illustrative example.

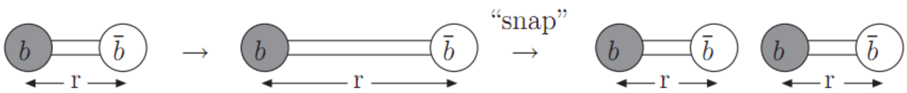

Figure 2.1: *A scenario that shows quark confinement. As the two quarks are pulled apart, two new quarks are created, leaving two hadrons instead of two free quarks [10].*

However, if heated to a critical temperature of approximately 2×10^{12} K, and at a critical density of approximately 1 GeV/fm^3 [11], matter undergoes a transition from a hadronic state to a QGP, where the quarks and gluons are *deconfined*. Study of the QGP at RHIC suggests that it behaves like an ideal fluid, in fact, it may be the most perfect fluid ever studied in a laboratory [12, 13].

2.1.2 Production In Heavy Ion Collisions

When heavy ions collide, such as gold at RHIC, or lead at the LHC, the ensuing fireball develops into a QGP via various different stages; as shown in Figure 2.2.

As the ions approach each other they suffer from length contraction due to the relativistic nature of the collision. This produces a *colour glass condensate (CGC)*, which can be imagined as a thin sheet containing a very high density ensemble of gluon states. The two sheets then for a brief moment become interlocked with one another, known as the initial singularity. Following this, as the sheets pass through each other, colour flux lines materialise between the two as shown in Figure 2.3, forming what is known as a Glasma. As time progresses, the Glasma evolves into a QGP which then finally ends as a hadron gas [14]. The label *sQGP*, simply refers to the fact that some theorists like to call this state the *strongly coupled* Quark Gluon Plasma [12].

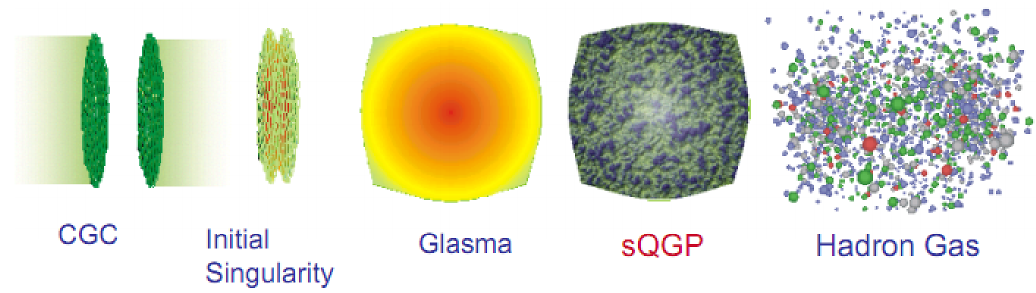

Figure 2.2: *The evolution of a heavy ion collision. Emissions from the different stages are believed to explain the ridge seen at RHIC, and thus a possible similar process could explain the CMS ridge in pp collisions. [14].*

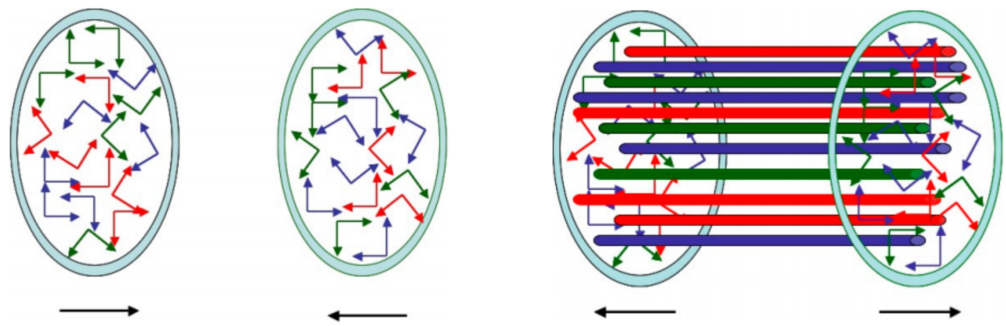

(a) CGC

(b) Formation of the Glasma

Figure 2.3: *These two figures represent the evolution from the colour glass condensate stage of the interaction to the formation of the Glasma.*

The ridge which was observed at RHIC, discussed in Section 1.2, is actually believed to originate from the colour flux strings in the CGC stage of the interaction [7]. There are encouraging studies that indicate the ridge originates from the super fluid properties of these matter states (for example, elliptical flow) which are believed to give rise to the ridge, with hydrodynamical studies of the evolution providing promising results [15, 16]. In any case, there seems little doubt that the creation of the heavy ion ridge does indeed coincide with the process of the creation of a QGP.

The data recorded by the experiments at RHIC over recent years, have allowed the community to conclude that QGP has indeed been produced [17]. A full description of techniques used to detect QGP can be found in reference [17]. Excluding two-particle correlations, these include techniques such as looking at the antecedently mentioned elliptic flow, and also jet quenching; this is where a parton which travels through the QGP may interact with its constituents causing it to lose energy. For example, this could be very noticeable in di-jet events where there is an imbalance in the energy of each back-to-back jet. In fact, ATLAS observed such a situation which was also dependent upon centrality, suggesting that a hot, dense medium was beginning to emanate from non-central collisions [18].

2.1.3 Role in the Early Universe

It is worth mentioning at this stage why QGP is currently a very important topic in physics. It is believed that a few microseconds after the Big Bang, the Universe was filled with a QGP. Recreating these conditions in the laboratory, allows the opportunity to study a state which is equivalent to this very early time. Observations on how it evolves and fluctuates could possibly shed new light on the evolution of the Universe as a whole [19]. The ALICE experiment [20] located at the LHC, is the latest experiment dedicated to investigating heavy ion collisions, which includes studying the QGP. It is also a test of the knowledge and understanding of QCD.

2.2 Colour Strings

As discussed in Section 1.3, the main goal of this analysis was to investigate whether a ridge structure emerged when studying events that would not produce a QGP medium of any kind. Instead, events are considered which are likely to have colour strings forming between interacting partons and the remnant protons; the emissions from the break up of such a string being the cause of the ridge. These strings are exactly the type of strings described when discussing quark confinement in Section 2.1.1. At its simplest level, a pp interaction such as that shown in Figure 2.4 is considered, where two quarks interact by exchanging a gluon and thus also colour. These outgoing quarks then colour reconnect with their non-parent protons (because of colour neutrality), forming a string of strong colour field between them.

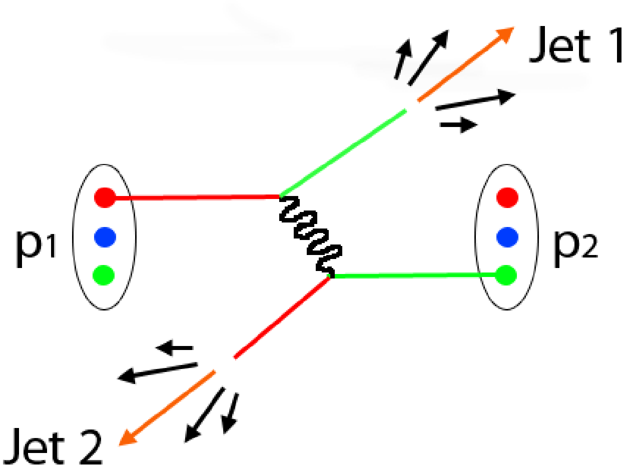

Figure 2.4: *Two quarks interact from the colliding protons, which exchange a gluon and thus also colour. A string would then form between jet 1 and the proton 2 remnant to colour neutralise, and likewise with jet 2 and the proton 1 remnant.*

2.2.1 String Enhancing Requirements

Cuts on events were implemented with the intention of enhancing the probability of strings being formed. Events which contained high energy jets were selected, which meant the jets themselves would be very forward in the detector. Hence, with the outgoing proton remnant travelling in the opposite η direction, this would maximise the length of any colour string connections formed. Therefore, this would hopefully enhance the amount of fragmentation which would contribute to the ridge.

Chapter 3

Methods of Analysis

3.1 Experimental Setup

3.1.1 The LHC

The data analysed in this investigation was provided by the Large Hadron Collider located at the European Organization for Nuclear Research (CERN) based in Geneva, Switzerland. At 27 km in circumference, it is the largest particle accelerator in the world today, and capable of the highest energies, where it is designed to be capable of 14 TeV proton-proton collisions at a luminosity of $10^{34}\ cm^{-2}\ s^{-1}$. It is widely expected that this accelerator will be the source of a new age in particle physics, with its potential for discoveries at these high energies.

On 30th March 2010, the first proton collisions at 3.5 TeV per beam took place, with the LHC running very successfully ever since. Collisions will continue at half the designed energy for rest of 2011 and during 2012. After a shutdown period, 2014 is expected to see the commencement of proton collisions at 13.5 TeV.

3.1.2 The ATLAS Experiment

Designed for general purpose studies, the ATLAS experiment is one of the four main detectors located at the LHC (the other three consisting of fellow general purpose detector CMS [21]; a focussed b-physics detector LHCb [22]; and finally a specialised heavy ion detector ALICE [20]). One of the main aims of the experiment is to complete the search for the infamous standard model Higgs boson. This search was used as a benchmark to define the performance of important systems in ATLAS. Along with the Higgs, results are hoped to answer questions in the topics of: dark matter, extra dimensions, supersymmetry, matter - anti-matter asymmetry and of course, discover some new unknown physics. A cut-away view of the ATLAS detector can be seen in Figure 3.1.

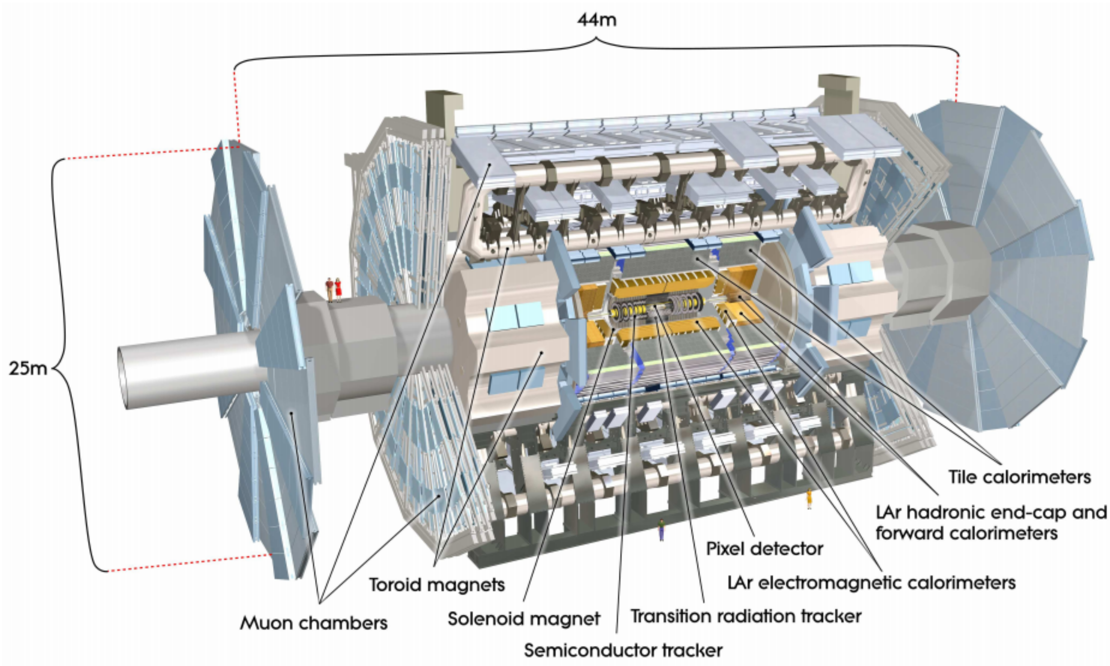

Figure 3.1: *A cut away view of the ATLAS detector. The total mass of the detector is approximately 7000 tonnes.*

The detector consists of three main detection components: the inner detector; the calorimeters; and the muon spectrometer. These are built up in cylindrical layers around the interaction point, as well as the two end caps. Two magnet systems are also installed to provide magnetic fields for the inner detectors and muon spectrometer. Below is a brief outline of these components [23, 24]:

3.1.2.1 Detector Components

- **Inner detector** - This is composed of firstly, a Pixel detector, followed by the Semiconductor Tracker (SCT) and finally the Transition Radiation Tracker (TRT). The main job of the inner detector is to record the particles position and momentum.
- **Calorimeters** - The LAr (liquid Argon) electromagnetic calorimeter is the inner most calorimeter which measures the energy of particles that usually interact via the electromagnetic interaction. Surrounding this are the hadronic calorimeters - measuring the energy of the particles that interact primarily via the strong force.
- **Muon Spectrometer** - The final section, surrounding all the other components, which measures the trajectory and calculates the momenta of muons produced by the collisions.

3.1.2.2 Magnets

The magnet systems, to allow for the bending of charged particles to measure their momentum, consist of the following:

- **Solenoid Magnet** - This is aligned on the beam axis and produces a 2 T axial magnetic field for the inner detector.
- **Barrel Toroid** (also two end-cap toroids) - provide a magnetic field of approximately 0.5 T and 1 T for the muon detectors in the barrel and end-cap regions, respectively.

3.1.2.3 Trigger System

The ATLAS trigger system consists of three distinct levels; these are L1, L2, and the event filter. It works in a way that each trigger level refines those selections made at the previous level and, where appropriate, implements additional selection criteria.

Full and detailed information about the ATLAS detector can be found in reference [23].

3.2 Data & Selections

Details on the datasets used during the investigation can be found in Chapters 4 and 5, as they are specific to each half of the analysis.

After studying track multiplicity from different streams, the JetTauETmiss datastream was chosen to be used throughout the analysis. This was because it offered more statistics at the high end of the multiplicity scale, also, it had the obvious advantage of containing the jets that were of interest.

3.2.1 Track Selections

Track selections were mostly taken from reference [25] as these provided a good, solid basis to initiate the analysis from. Along with these, it was made sure that only tracks with a transverse momentum greater than 400 MeV/c were considered, analogous to the CMS study. These cuts were applied throughout the whole analysis with no changes. The complete set of track selections were:

- Pixel detector hits > 1
- SCT detector hits > 6
- $|\eta| < 2.4$
- $D_0 < 1.5$ mm

- $Z_0 < 1.5$ mm[1]
- Track $p_T > 400$ MeV.

Where D_0 and Z_0 are the longitudinal and transverse impact parameters respectively.

3.2.2 Event Selections

Event selections, covering quality and physics, consisted of the following requirements:

- Good Run Lists were always used.
- Jet cleaning was applied (more detail in following chapters)
- Pileup addressed
- Variable cuts on:
  - Sum of the transverse energy, E_T and total energy, E, of all the jets in the event.
  - Track Multiplicity.

Pileup was tackled by attaching each track to the nearest vertex, and then only using tracks from the primary. The z-positions of each vertex were then analysed, and if one was discovered to be within 10mm of the primary vertex, the event was rejected. It would have been possible to increase this cut, but 10mm still allowed for a good level of statistics, while at the same time keeping the worst effected events from being considered. Jets were reconstructed using the AntiKt4 algorithm [26], and calibrated using the electromagnetic (EM) scale.

3.3 Calculating the Two-Particle Correlation Function

The two-particle correlation function as a function of $\Delta\eta$ and $\Delta\phi$ which was used by CMS, and also by this investigation, is presented in Equation 3.1

$$R(\Delta\eta, \Delta\phi) = \left\langle (\langle N \rangle - 1) \left(\frac{S_N(\Delta\eta, \Delta\phi)}{B_N(\Delta\eta, \Delta\phi)} - 1 \right) \right\rangle_{bins} \quad . \tag{3.1}$$

Firstly, the complete sample was separated into 10 bins according to the track multiplicity of the event. This was implemented in such a way that each bin contained approximately the same number of entries. $\langle N \rangle$ is simply the average multiplicity value of the respective bin, and S_N and B_N are the signal and background distributions, which are defined in Equations 3.2 and 3.3 respectively. Finally $\Delta\eta = \eta_1 - \eta_2$ and $\Delta\phi = \phi_1 - \phi_2$.

$$S_N = \frac{1}{N(N-1)} \frac{d^2 N^{signal}}{d\Delta\eta d\Delta\phi} \quad . \tag{3.2}$$

[1]This cut was slightly different from the reference, which originally had a cut of $|Z_0 \sin(\theta)| < 1.5$ mm. When testing the data, pileup was a concern with the $\sin(\theta)$ term, thus it was removed with the intention of possibly revisiting and refining the cut if required.

$$B_N = \frac{1}{N^2} \frac{d^2 N^{mixed}}{d\Delta\eta d\Delta\phi} \quad . \tag{3.3}$$

The signal was produced by using particles from the same event, whereas the background was constructed by using mixed event pairs. Figure 3.2 below shows an example of each histogram, using early ATLAS data produced during the analysis. The order in which the particles are considered is insignificant, $\Delta\eta$ and $\Delta\phi$ are always taken as positive and then only one quadrant of the histogram was filled; the remaining three were filled by reflection.
The signal and background division was calculated first for each bin, with the weighting as seen in Equation 3.1 being applied. These were then averaged over to acquire the final result. The same method was applied to calculate the two-particle correlation function in the cases of both the pp and Pb-Pb collisions.

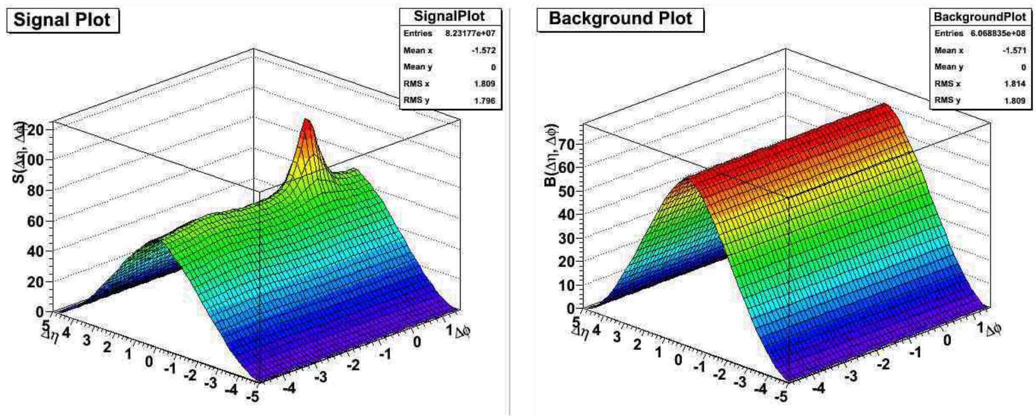

Figure 3.2: ***Left:*** *A signal plot from ATLAS data described by Equation 3.2.* ***Right:*** *A background plot also produced from ATLAS data as described by Equation 3.3. The signal plot is then divided by the background plot to obtain the two-particle correlation plot.*

Chapter 4

Release 15 - Data, Results & Discussions

4.1 Collision Data

During the first stage of the investigation, datasets from four periods[1] were analysed and are described in Table 4.1 below. These were produced with release 15 software[2].

Period	Luminosity (pb^{-1})	Number of Events
F	1.98	60×10^6
G	9.1	
H	9.3	36×10^6
I	23	

Table 4.1: *Shows the periods and their respective luminosities used in the analysis. Details on ATLAS data periods can be found in reference [27].*

In real time, the data included in periods F & G was collected between mid-August to early October 2010. The remainder of October saw the collection of the periods H & I data. Jet cleaning in this data was handled by 3 variables: 'JetIsGood', 'JetIsBad' and 'JetIsUgly'; only jets with the JetisGood tag were considered in the analysis. Data from Periods F & G were the first to be analysed, with H & I being added later, as explained in the following sections.

[1]The data that is collected by ATLAS throughout the year is divided into different periods. Each run that is intended for physics analysis is assigned a period and subperiod, e.g. E4. It is designed in a way that a period of data should have similar settings and detector environments. Any major changes to triggers or detector calibration usually results in a new period. See reference [27] for more information.

[2]An ATLAS release simply refers to the version of the software used to process the raw data collected from the detector. The data analysed in this chapter was processed with release 15 of the software in 2010, where as the data analysed in the following chapter was re-processed using release 16 software. Each iteration improves on the last, providing bug fixes, better calibration and incorporates enhanced detector understanding.

4.1.1 Triggers

What has not been mentioned up until this point is the role of triggers. This initial half of the analysis was performed with a mix of triggers, which meant that no specific triggers were selected to analyse. The reasoning for such a decision was because of the assumption that the very forward jets that were of interest (refer to Section 2.2.1) should be triggered, regardless what mixture of triggers were running.

4.2 Results & Discussion

4.2.1 Equivalent to CMS Cuts Analysis

Firstly, an attempt was made to recreate CMS's analysis as closely as possible, to investigate whether a structure could also be seen in the same environment, but in ATLAS data. If a ridge structure was seen, then the possibility that the CMS ridge was in fact the result of a string effect could be investigated. To perform this analysis, cuts were implemented of multiplicity $N > 110$ and the sum of the transverse energy, E_T, of all the jets > 60 GeV (a rough equivalent of the total energy deposited in the calorimeter). Only tracks within the p_T range of 1 GeV/c - 3 GeV/c were analysed, with the data consisting of events recorded during periods F & G.

Figure 4.1 shows the result of this analysis, where no structure was observed in the ridge region. Even though, the ridge being absent was still interesting, ATLAS simply did not have the same amount of high multiplicity events recorded as CMS, so no conclusions could be drawn from this result.

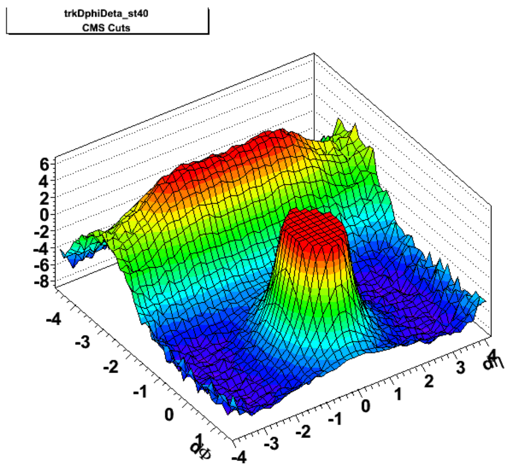

Figure 4.1: *This shows the resultant 2-D two-particle correlation plot from the analysis of performing cuts similar to the CMS study. Events from periods F & G were analysed.*

4.2.2 String Effect Search - Periods F & G

Attention was turned to investigating the hypothesis of string fragmentation being a possible source of the ridge. Hence, the data was now analysed requesting that the sum of the total energy of all the jets was quite high, in order to look at forward jets. No cuts were placed regarding the jet E_T. The evolution of such requests on the jet energy can be seen in Figure 4.2. The multiplicity was kept at $N > 110$ in each case, with the track p_T between 1 GeV/c - 3 GeV/c.

Plot 4.2(a), with a cut of the sum of the total jet energy > 900 GeV, did not show any signs of a ridge at all, but as the cut was raised to 1.6 TeV, and then onto 2.4 TeV, in plots 4.2(b) and 4.2(c) respectively, there were hints that something was materialising in the ridge region. In the final plot, 4.2(d), a clear ridge-like structure emerged when the cut on the total energy was increased to 2.8 TeV. However, what was also evident in the progression of these cuts was that the statistics were beginning to become quite poor, as viewed by the spiky nature of the latter plots compared to the first. Increasing the cut from 900 GeV to 2.8 TeV loses 89,177 events in the process, and because of this; statistical fluctuations could not be completely ruled out as being the source of the newly observed structure. Nevertheless, it seemed to somewhat resemble what was observed in the CMS result.

At this early stage of the analysis, it was not possible to determine whether this was a valid signal or a fluctuation, but was a promising lead nonetheless. Hence, to improve on the statistics side of the analysis, newly available data (at the time) from periods H & I was incorporated into the analysis.

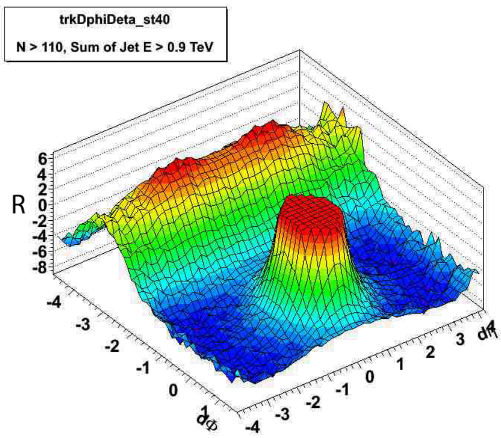

(a) > 0.9 TeV

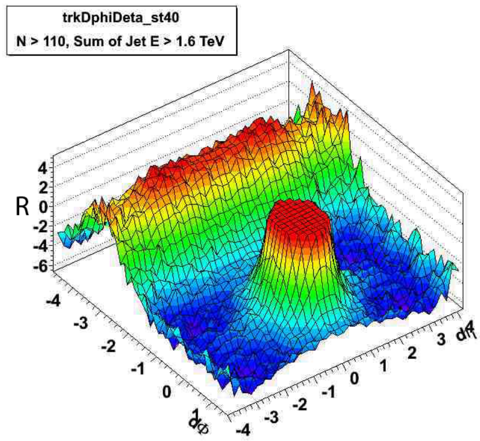

(b) > 1.6 TeV

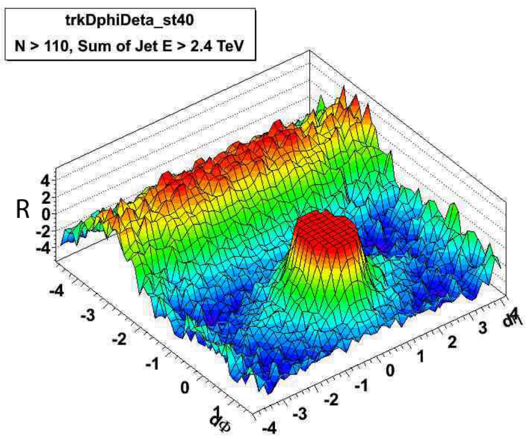

(c) > 2.4 TeV

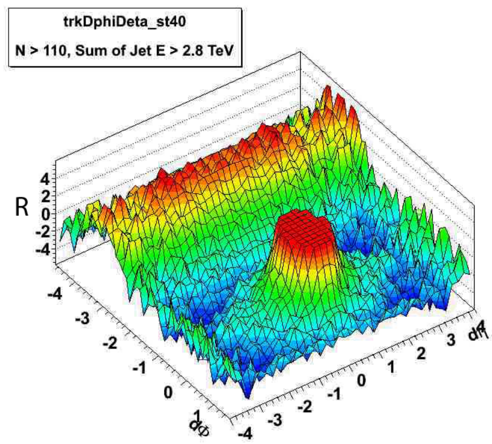

(d) > 2.8 TeV

Figure 4.2: *This presents the results of the F & G data analysis, all requesting multiplicity of over 110 tracks along with (a) sum of the jets' energy greater than 0.9 TeV where 110 287 events passed the cuts, (b) sum greater than 1.6 TeV where 59 597 events passed, (c) sum greater than 2.4 TeV where 29 805 events passed and (d) sum greater than 2.8 TeV where 21 110 events passed the requirements. Structure appears to emerge, especially in (d), when requesting these high sum of jet energies.*

4.2.3 Periods H & I

It was now known where to search for a ridge feature, thus the same cuts that proved successful with the F & G data were applied to the continuing analysis. Figure 4.3 shows the results, where plot 4.3(a) displays purely the result from the periods H & I data only, and then plot 4.3(b) presents the outcome of having included the H & I data with the F & G data (plot 4.2(d)). It was instantly striking that adding the H & I data in fact had a negative effect on the ridge. When analysed on its own, no ridge was apparent, there was some sort of structure around the region, but this was perhaps a fluctuation highlighted by the symmetric nature of its construction. When added to the F & G data, whilst making the result slightly smoother, the ridge effect which was previously seen, was simply reduced. There were two possible scenarios that could explain what had been observed:

- There was simply no signal at all, and that which was seen in periods F & G was the result of fluctuations that happened to manifest in the ridge region.
- Trigger changes between the two period sets may have been responsible. The assumption that the very high energy jets would be triggered efficiently was possibly false, with the events that gave rise the ridge in F & G being lost in H & I. Figure 4.4 shows a possible hint of a difference, by looking at and comparing the the E_T spectra of the two sets of periods. It shows just enough deviance to suggest that this could be the reason for the ridge disappearance.

However, there was one check that could be performed to try and validate whether the ridge seen in F & G was a true signal.

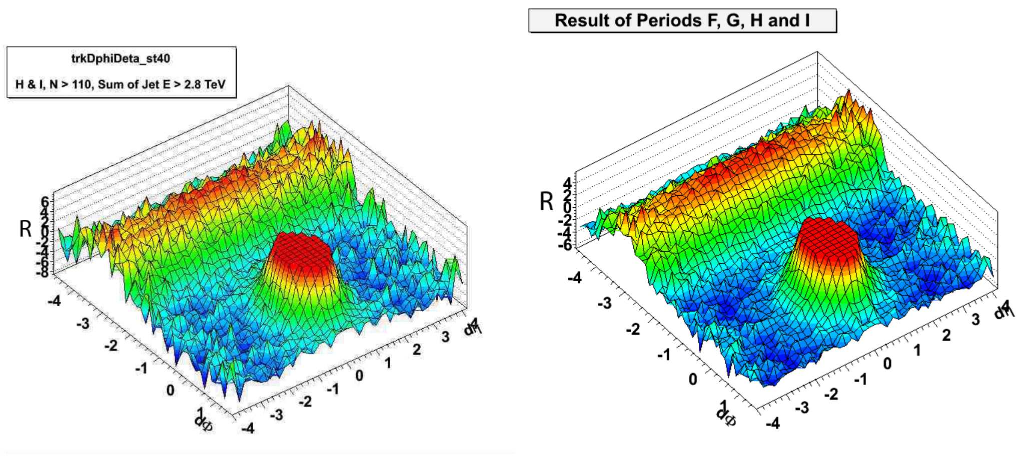

(a) Periods H & I Only

(b) Periods F,G,H & I

Figure 4.3: *This shows the results of (a) analysing the data from periods H & I, with 16,445 events passing the cut of multiplicity above 110 and sum of the total jet energies greater than 2.8 TeV. Then (b) displays the result of when the H & I data is combined with the data from F & G, with a total of 37, 555 events passing the requirements.*

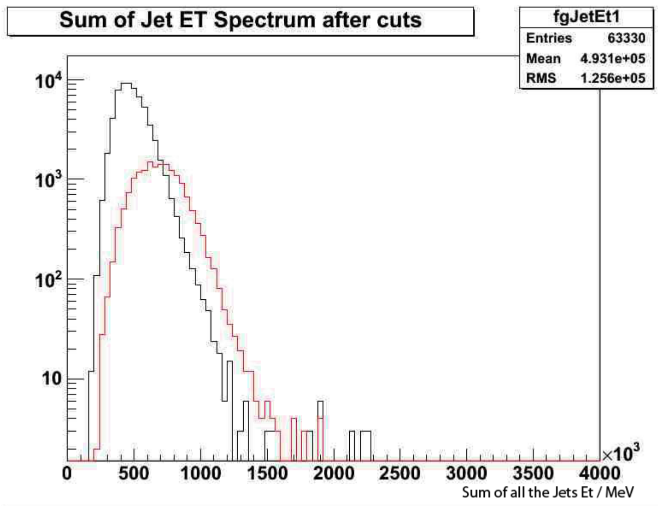

Figure 4.4: *This shows the difference between the E_T spectra of the F & G data, and the H & I data. The H & I data has been scaled for the relative luminosities.*

4.2.4 Mixing the p_T Range

The check performed involved mixing the track p_T between each pair of tracks. The investigation so far had only considered tracks within the p_T range of 1 GeV/c - 3 GeV/c, partly because this is the range where CMS observed a ridge. Outside of this range, it was claimed that a ridge structure was not seen. There was also the need to check that the cuts had not been specifically tuned to see the ridge, and to ensure that they had not maximised a statistical fluctuation wich was subsequently interpreted as the ridge. If it was truly just statistics, then when looking at a different set of data, which would be obtained by pairing the tracks with a different track from a different p_T range, then no ridge should be seen.

To achieve this, the track p_T selection window was expanded to 0.7 GeV/c - 5 GeV/c. The analysis was performed as normal, but when a track with a p_T in the range of 1 GeV/c - 3 GeV/c was selected, it was not allowed to be paired with a track in the same range. This made sure that a different set of data, although close to the original, was entered into the correlation calculation. Only the data from periods F & G was analysed, as of course H & I showed no ridge to confirm.

Figure 4.5 shows the 2-D correlation plot of mixing the p_T ranges. Although still quite noisy, and the value of the overall $R(\Delta\eta, \Delta\phi)$ being reduced, a ridge structure is still visible. This pointed towards the finding in this dataset as being a valid effect.

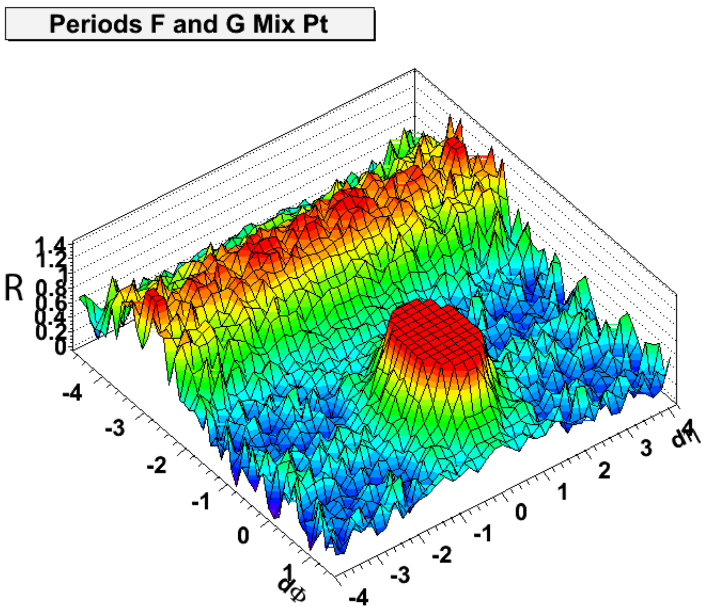

Figure 4.5: *This displays the result of the normal two-particle analysis but with the mixed* p_t *method applied. The cuts of the sum of the total jet energy* > 2.8 *TeV, and* $N > 110$ *were still in place. Although quite short on statistics, a ridge structure remains visible.*

Even with this result from the mixed p_T analysis, the fluctuations were still very present and important in the plots, so at this point it had become important to understand the errors associated with the analysis.

4.2.5 Errors

The errors were calculated by assuming that for each $\Delta\eta$ bin in the background plot (refer back to Section 3.3 for an example of the background plot) each $\Delta\phi$ value should be equal. So from this, a simple standard deviation error was calculated for 'strips' of $\Delta\eta$ and applied to each bin in $\Delta\phi$. The same errors were then applied to the signal plot with the assumption that the actual signal makes up a very small fraction of the complete plot, thus meaning that the error could be assigned in this way. These errors were then propagated through the calculation of $R(\Delta\eta, \Delta\phi)$.

Figure 4.6 presents the errors calculated in each $\Delta\eta$ bin, for the plot seen in Figure 4.2(d), the period F & G ridge plot. While the detector coverage allowed measurements of $|\Delta\eta|$ up to a value of 5, the plots presented here and indeed those by CMS, all cut at $|\Delta\eta| = 4$. The error plot in Figure 4.6 demonstrates that in the region $|\Delta\eta| > 4$, the errors increase substantially compared to the rest of the plot, thus, this region was simply not trusted. The errors otherwise seemed quite acceptable, and remained so when future results were evaluated.

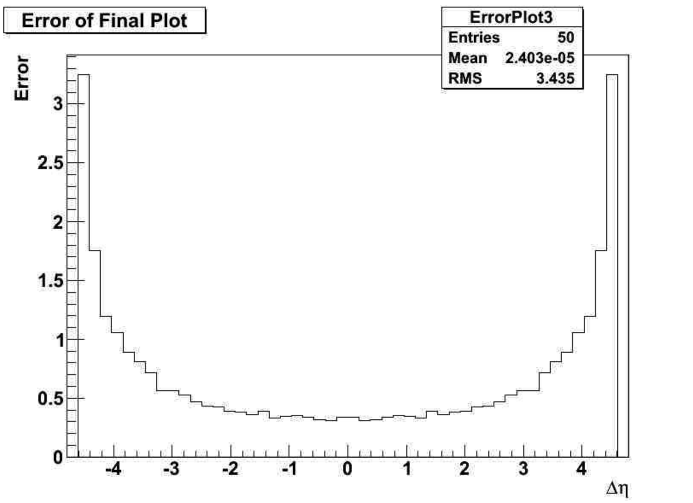

Figure 4.6: *This histogram displays the errors for the plot seen in Figure 4.2(d). Note how the errors beyond $|\eta| > 4$ rise very rapidly; this makes this region quite unreliable for detecting a signal, so only $|\eta| < 4$ values are trusted in the results.*

4.2.6 Fitting

With errors now applied to the results, the possibility of fitting a model was investigated. The first attempt was performed by using a relatively popular model for ridges observed in heavy ion data, the function for which can be seen below in Equation 4.1 [28]:

$$\frac{\Delta\rho}{\sqrt{\rho_{ref}}} = A_0 + A_1 e^{-\frac{1}{2}\left\{\left(\frac{\phi_\Delta}{\sigma_{\phi_\Delta}}\right)^2 + \left(\frac{\eta_\Delta}{\sigma_{\eta_\Delta}}\right)^2\right\}} + A_2 e^{-\frac{1}{2}\left(\frac{\eta_\Delta}{\sigma_2}\right)^2} + A_D[1+\cos(\phi_\Delta - \pi)]/2 + A_Q 2\cos(2\phi_\Delta) \quad . \tag{4.1}$$

The A_0 term in Equation 4.1 defined the baseline of the plot; the A_1 term described the near-side jet peak; the A_2 term was for the slight Gaussian curve that stretches in $\Delta\phi$ centred at $\Delta\eta \approx 0$; the A_D term described the far side ridge; and finally the A_Q term modelled the ridge. However, an altered version of the model was also tested, where the ridge was described as a Gaussian instead of a cosine. This change was made because firstly; a Gaussian may have provided a better description and secondly; there were concerns about simply fitting the ridge with the away side shape and changing its name. Thus, the last term was modified to become:

$$A_Q e^{-\frac{1}{2}\left(\frac{\phi_\Delta}{\sigma_2}\right)^2} \quad . \tag{4.2}$$

The fitting was applied to the F & G data which displayed the ridge structure, with Figure 4.7 showing the result.

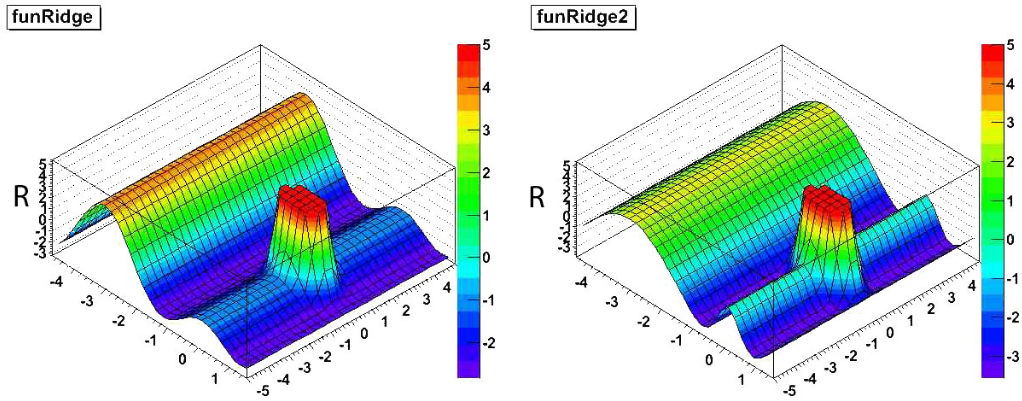

Figure 4.7: *This displays the result of fitting the model as shown in Equation 4.1, to the period F & G analysis which showed structure, with the ridge described by* ***Left:*** *a cosine and* ***Right:*** *a Gaussian. While the Gaussian appeared to be a stronger description, the quality of the fits are not very good as shown below in Table 4.2.*

Ridge Fit Type	Ridge Fitting Value	Error	χ^2	Per degree of freedom
Cosine	1.95	0.03	15640	6
Gaussian	5.04	0.07	26238	10

Table 4.2: *This shows the results of the fitting seen in Figure 4.7. The ridge seemed much stronger when described by a Gaussian function.*

Whilst the results seemed to indicate the existence of the ridge, the fit at this stage was simply not very good, as evidenced by the χ^2 and per degree of freedom values in Table 4.2. Additional caution was applied to the fitting due to the symmetrical nature of results construction.

4.2.7 The Next Steps

These early results indicated that there was perhaps some sort of effect, similar to the CMS ridge, being produced in these very high energy jet events. Data from periods F & G seemed to show a ridge-like structure, even when analysed with the mixed p_T method. However, on the other hand, periods H & I showed no similar results - it had seemed like the ridge had disappeared. It was concluded that trigger inconsistency may be the source of the discrepancy, which meant that the events that were contributing to the ridge in the F & G data, were possibly not being selected in periods H & I.

The primary aim from this point onward was to investigate the triggers that were running in each dataset, and attempt to and establish which trigger (or triggers) were contributing to the ridge. With this there were two possibilities: firstly the triggers which acted as the source of the ridge were simply not active in the later runs; or secondly, other triggers were swamping the ridge signal; meaning that it could be likely that the ridge could be observed in H & I by constructing the correct trigger cuts. This was continued in the second half of this study.

4.3 Heavy Ion Analysis

The late 2010 Pb - Pb collisions at the LHC presented an opportunity to examine heavy ion data first hand, partly to study whether a ridge could be observed in a high parton density environment where a ridge would be expected. This chapter closes with a brief look at this analysis, which conjured up its own intriguing results.

4.3.1 Data & Method

The data consisted of 224,120 events from Pb-Pb collisions at $\sqrt{s_{NN}} = 2.76$ TeV. During the run, a peak luminosity of $6.4 \times 10^{24}\ cm^{-2}\ s^{-1}$ was achieved.

The method for analysing the data remained the same as that for pp; the data was binned according to the the multiplicity of the events, and the only cut left over (admittedly, for not any particular reason) was that of multiplicity being more than 110 tracks. However, one extra parameter was added as this was to calculate the centrality of the event.

4.3.2 Results

Figure 4.8 shows the basic result obtained and is simply the 2-D two-particle correlation function for the heavy ion data. It was somewhat relieving to observe that a ridge was indeed produced, and was in fact very distinct, indicating that a QGP-like substance was created in the heavy ion collisions recorded by ATLAS. It was reminiscent of the RHIC ridge discussed in Section 1.2.

A further analysis was performed where each bin was taken separately, the boundaries of which can be seen in Figure 4.9, and calculated their respective centralities. Figure 4.10 shows four bins from this process; bins 0, 3, 6 and 9, the details of these bins can be found in Table 4.3.

Bin	Centrality	Mean N
0	0.89 – 1	168
3	0.51 – 0.60	649
6	0.25 – 0.34	1425
9	0.00 – 0.05	3326

Table 4.3: *This table shows the details the four bins whose results are shown in Figure 4.10.*

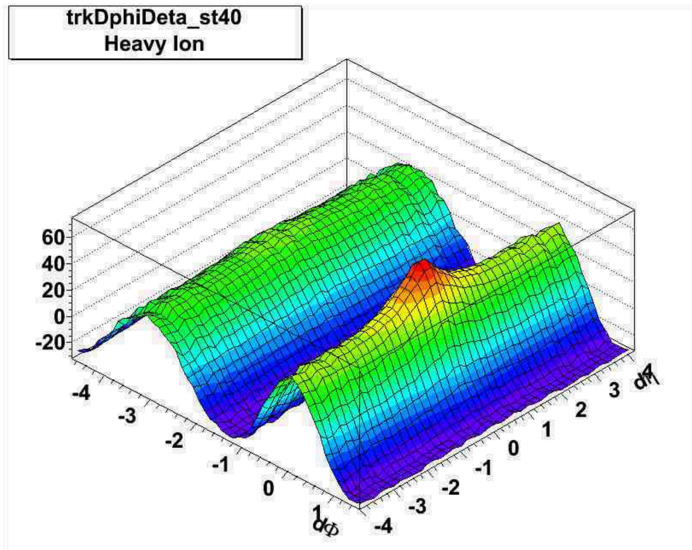

Figure 4.8: *The Pb-Pb collisions produced a very significant near side ridge as seen in this plot. It was comparable even with the away side ridge. 30,665 events passed the requirements.*

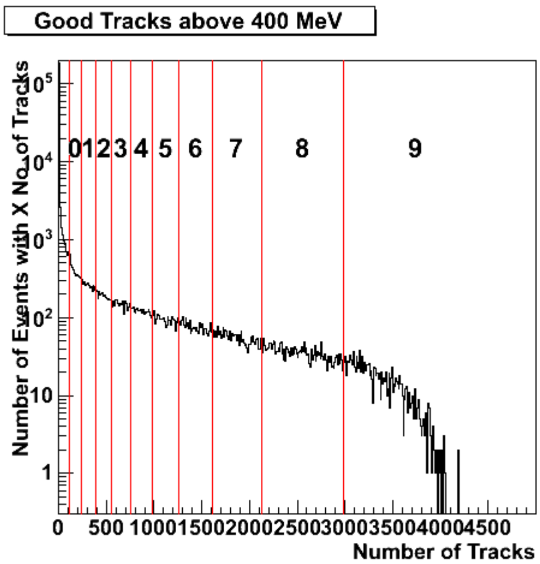

Figure 4.9: *This plot displays the boundaries of the ten bins, based on track multiplicities, used in the heavy ion analysis.*

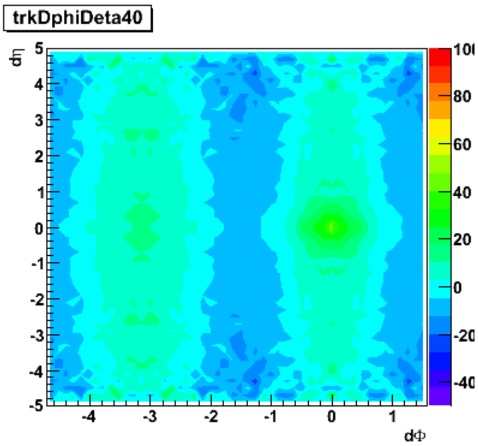

(a) Bin 0 - High Centrality

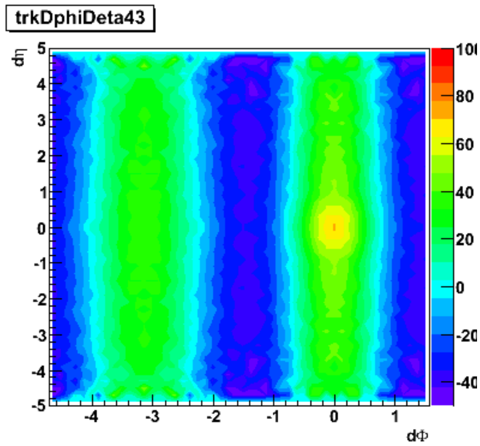

(b) Bin 3

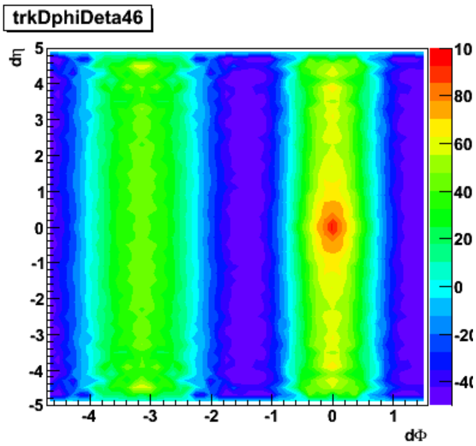

(c) Bin 6

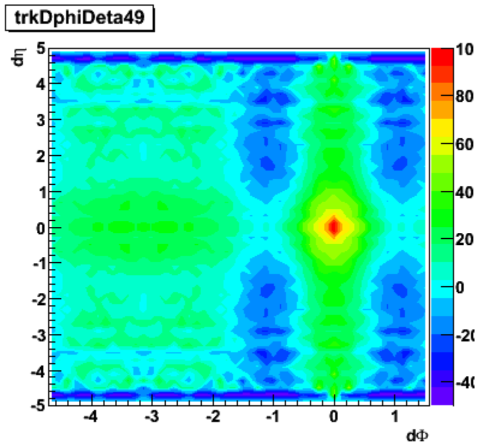

(d) Bin 9 - Low Centrality

Figure 4.10: *This shows the resultant plots of the four bins, the information for which can be found in Table 4.3. Bins 0 through to 6 all look roughly similar, however in bin 9, the away side ridge suddenly becomes $\approx \pi$ in width, suggesting something peculiar is happening to the jets when the collisions are at low centralities.*

What was found was that whilst the first three plots looked quite similar and displayed normal features such as both ridges and the jet peak, when bin nine was examined, which meant a low centrality, the away side ridge appeared to smear out to about a width of π. This seemed interesting, as it implied that at low centrality, where current evidence implies that a QGP substance is very likely to be produced, the jets were being affected by some process and were being caused to spread out over ϕ in the detector. A possible reason for this could be jet quenching, and it seemed possibly related to the previously mentioned *centrality dependent di-jet asymmetry* observed by ATLAS [18].

While a very interesting study, the analysis of the heavy ion data was concluded at this point, with it being very pleasing to see that the method and analysis did indeed detect the ridge phenomenon.

Chapter 5

Release 16 - Data, Methods, Results & Discussion

5.1 New Reprocessed Data

In order to investigate the triggers the same data was obtained in a different format, and in parallel, the opportunity was used to switch to newly available reprocessed data, made with the updated release 16. This meant improved calibration and many bug fixes. Access to the full 2010 dataset was now also available, although with the JetTauEtmiss data stream only being available from period E onwards, data from the L1Calo steam was used to provide the rest. The full set of data and details can be found in Table 5.1.

Datastream	Period	Luminosity (nb^{-1})
L1Calo	A	0.4
	B	9
	C	9.5
	D	320
JetTauEtmiss	E	1.12×10^3
	F	1.98×10^3
	G	9.1×10^3
	H	9.3×10^3
	I	23×10^3
Total Luminosity		44×10^3

Table 5.1: *This table displays the data available to process in the second half of the investigation. The total number of events contained in these datasets was* 2.61×10^8.

Jet cleaning was also vastly improved in this release with full details found in Appendix A.

When the new data was first examined, it was discovered that the cut from the previous analysis (requesting that the sum of the total energy of the jets be greater than 2.8 TeV) was allowing very few events through. On closer inspection, a significant difference was found in the spectrum of the total jet energy sum between the old and the new data, which is shown in Figure 5.1. The new data spectrum looked a lot cleaner than its predecessor, and was an example of how the new dataset is a big improvement over the old, in terms of quality. It was also decided to remove jets with an $\eta > 4.5$ as these were simply not trusted in ATLAS analyses.

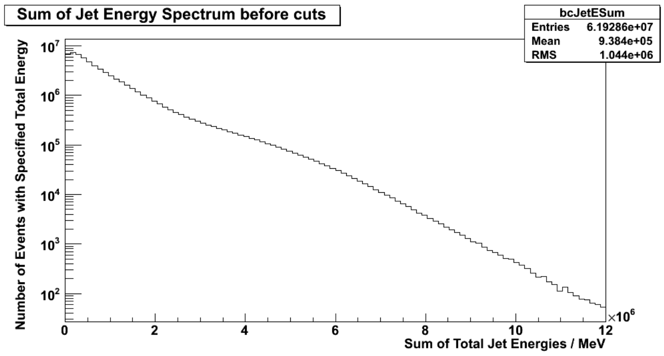

(a) Release 15 Spectrum

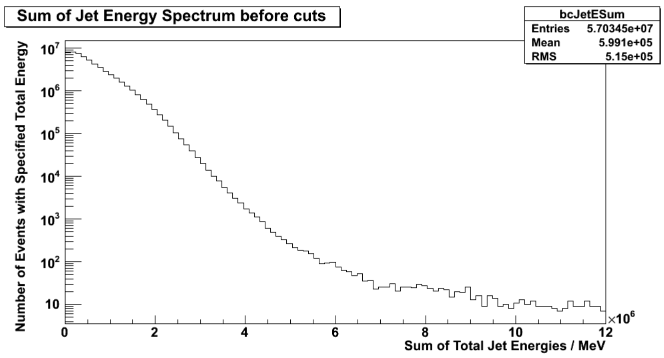

(b) Release 16 Spectrum

Figure 5.1: *This shows the difference between (a) sum of the total energy of all the jets spectrum from release 15 data and the same in (b) but from release 16. Both are from Periods F & G, difference in entries may come from better good run lists. Note that the y-axis is on a log scale and no jet cleaning had been applied to the data.*

5.2 Method of Trigger Investigation

The main reason for moving to the new dataset was to acquire access to the trigger information, and this was now available. It was decided to use event filter level triggers (refer back to Section 3.1.2.3 for information on the ATLAS trigger system) for the analysis, and decided to actively look at every trigger in the data stream. Whilst there were particular triggers that could have been selected as being useful to the investigation, such as jet specific and total energy triggers, it was not known whether these were really the ones that were contributing to the ridge. Any trigger could in fact contribute meaningfully, hence the decision to analyse them all.

While different rates were expected, it is also worth mentioning that the trigger was not static throughout the time line of the data collecting (which was partly the suspicion of the ridge disappearance). The first big difference came from the switch in different streams; the transition from L1Calo to JetTauEtmiss. While there are similar triggers in each, they are not the same and some triggers were dropped in favour of others. This was to be expected however, and since the analysis up to this point had not included data from periods A - D, this was not dwelled upon. There was one change however that impacted the analysis slightly; apart from normal and expected removal and addition of triggers. In periods E and F only level 1 in the trigger system was rejecting events, but from period G onwards level 2 also started to reject events based on the running triggers. This meant a change in naming structure and some differences in rates. One further change was noticed and this was an addition of a dozen triggers in period H designed for a different analysis; this is highlighted due to the fact that it occurs within the period of interest where the ridge structure vanishes, and changes like this could have had an impact.

Each trigger was presented in the data as either being on or off, and to monitor the triggers the following method was implemented. First of all, a count was initiated of exactly how many pairs of tracks were being entered into the ridge region by each event. This region was defined by the values: $2.0 < |\Delta\eta| < 4.0$ and $|\Delta\phi| < 0.7$, and the same monitoring was installed in the creation of the background plot, so it was known how many tracks were entering both the signal and background ridge region. The following ratio was then calculated from these values:

$$A = \frac{2P_{Ridge}}{N_{Total}(N_{Total} - 1)} \quad . \tag{5.1}$$

Where P represented the number of pairs of tracks, with N the total number of single tracks. Next, for each trigger, a profile histogram was created consisting of two bins. When the trigger was triggered in the event, bin one was filled with ratio A. If the trigger was off for that event, then the ratio was entered into bin two. What this allowed was to quickly analyse and identify triggers that were contributing to the ridge, as the first bin average, meaning when it was triggered, would be noticeably higher than its second bin counterpart. Figure 5.2 shows an example of such a plot.

The error bars on the average provided an indication of the number of events associated with the respective trigger. For example, a very large error bar would mean that very few events are associated with that particular trigger. Or if there was no error present, although it seemed good, meant that only one entry had been made and should really be ignored. In conjunction to the ratio analysis, a simple plot of each trigger rate for the events was also recorded.

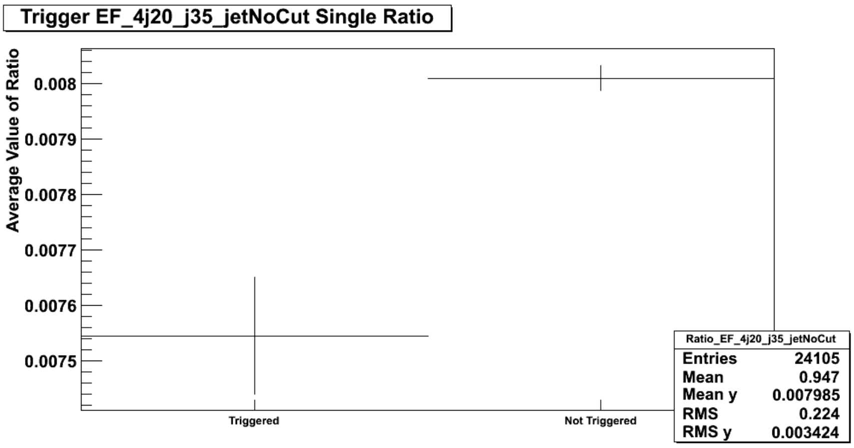

Figure 5.2: *The profile plot provided an easy way to see if a trigger contributes to the ridge or not. In this case bin one is much lower than bin two so it can be said that this is not a ridge contributing trigger. Indeed this example could be interpreted as an anti-ridge trigger, with many more events contributing to the background. Most were expected to be roughly even. The error bars in this example also indicate that there is a decent amount of events with this trigger.*

5.3 Results & Discussion

Naturally the first task of analysing the new data was to investigate whether the suspected ridge was still observed. Hence, some analyses that were performed in the last chapter were re-performed at this stage, and are presented in the following sections.

5.3.1 Periods F & G

As discussed in Section 5.1, not many events were passing the original cuts. Thus, in an attempt to recreate the previously observed ridge, the requirement on the sum of the total jet energy was varied, until a similar number of entries were being allowed through as there were in release 15 ($\approx$ 21,000). This was because even though the jet energy spectrum had been improved, the multiplicity was the same between the two sets of data. Figure 5.3 shows the evolution of the correlation when increasing this cut. Similar to the previous analysis, there was nothing to observe in the low cut requirement plots as seen in 5.3(a) and 5.3(b), it's only when the cut is higher that there was a hint of a structure. Plot 5.3(c) with a total jet energy cut of 1.3 TeV exhibits some change in the ridge region, and contained the closest number of events to the release 15 data, with 20,861 events entering the result. Whilst it was nowhere near as definite as the structure which was seen with the release 15 data, plus a few strange dips here and there, it was possible to pick out certain features. However, it could not be denied that this result cast a little doubt over the validity of the observed ridge. Increasing the cut by 0.4 TeV to 1.7 TeV, vastly decreased the statistics, as evidenced by 5.3(d). Although, it did indeed contain some structure in the ridge region, it was not in the form of a ridge, and was far too noisy to draw a conclusion from.

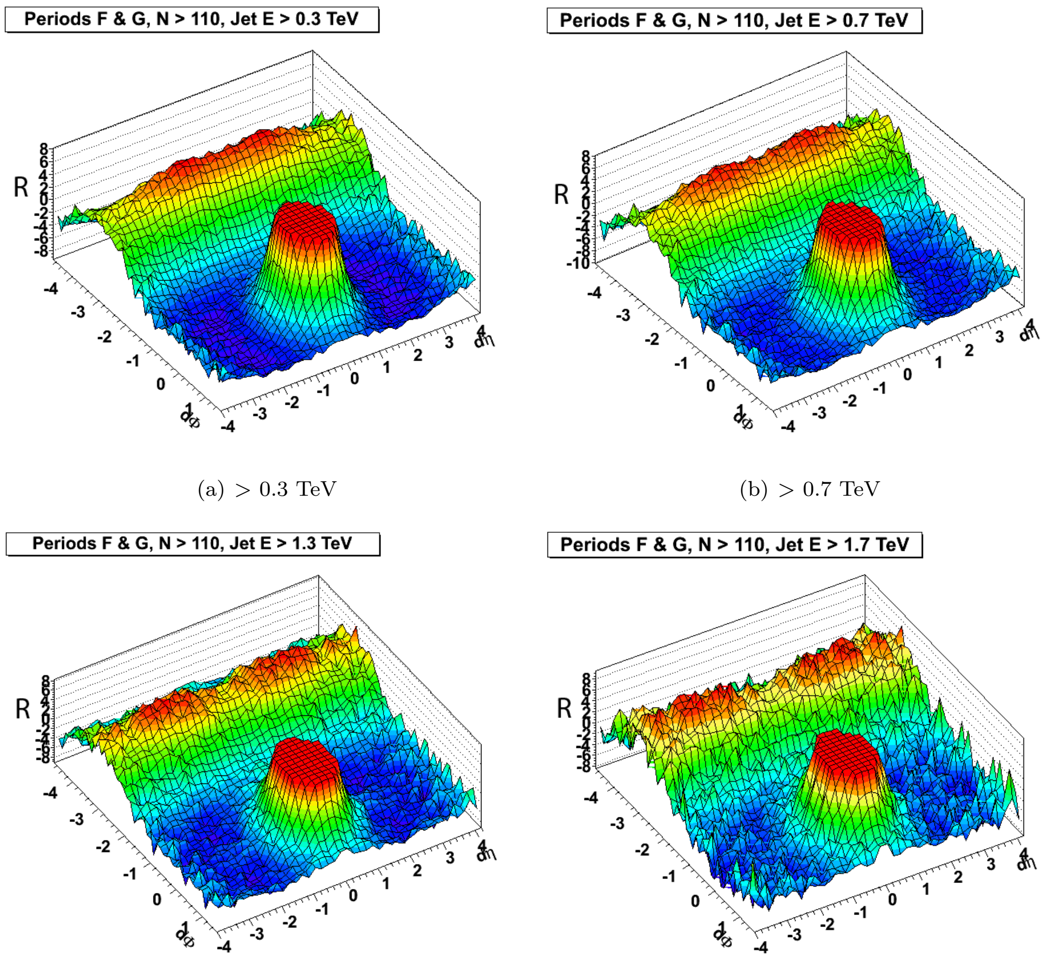

(a) > 0.3 TeV

(b) > 0.7 TeV

(c) > 1.3 TeV

(d) > 1.7 TeV

Figure 5.3: *This presents the results of the F & G data analysis on the new release 16 data, all requesting multiplicity of over 110 tracks along with (a) sum of the jets energy greater than 0.3 TeV where 82,551 events passed the cuts, (b) sum greater than 0.7 TeV where 59,585 events passed, (c) sum greater than 1.3 TeV where 20 861 events passed and (d) sum greater than 1.7 TeV where 8910 events passed the requirements.*

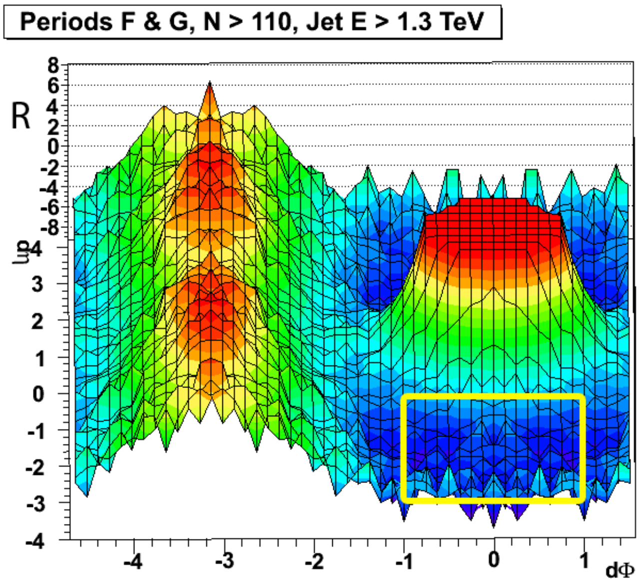

(a) > 1.3 TeV

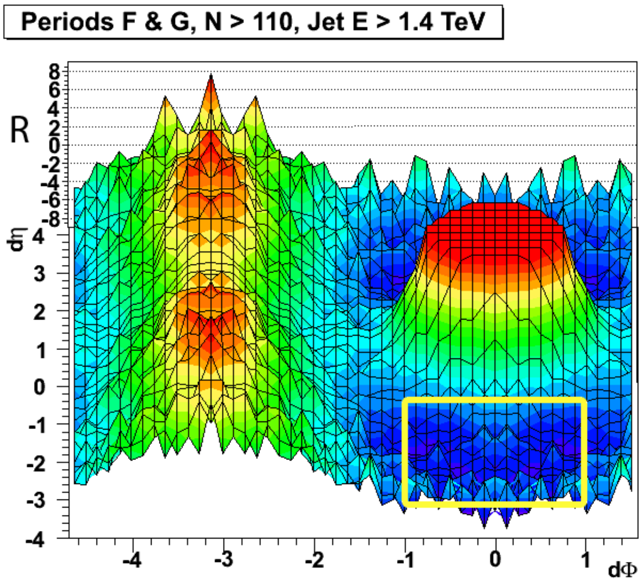

(b) > 1.4 TeV

Figure 5.4: *Presented here is a side view of the 2-D correlation plots, both with a multiplicity cut of 110 tracks, but with the cut on the sum of the total jet energy being (a) greater than 1.3 TeV, and (b) greater than 1.4 TeV. There still appears to be a hint of a structure in the ridge region.*

Figure 5.4 displays a side on view of the 2-D correlation, with 5.4(a) showing the plot from 5.3(c) and then 5.4(b) shows the result of the cut being raised by 0.1 TeV to 1.4 TeV. As highlighted in the figures, from this view there appeared to be a definite general rise and fall in the ridge region, but as mentioned, certainly not as pronounced as previously observed. What is also noticeable in all these plots, not just some as previously observed, but has remained unmentioned up until this point, is the two-humped nature of the away side ridge. It was believed that this was just a consequence of looking at high energy jet events, where the jets themselves are more likely to be found at relatively forward angles in the detector.

5.3.1.1 Mixing the p_T

In light of what had just been observed, the same test that was performed previously was applied; by mixing the p_T of the track pairs and not letting two from the range of 1 GeV/c - 3 GeV/c be paired together. The result, as shown in Figure 5.5, displayed no extended ridge structure. It had a strange extension at the base of the peak, however no extension beyond this. Naturally this cast doubt over the results previously seen. The test was designed to validate any observed ridge as not being a result of fluctuations, thus this pointed towards the ridge not being a true signal.

However, there was a significant and very real difference between the two sets of periods in the previous set of data, so the investigation continued to discover whether this difference was still present in the release 16 data.

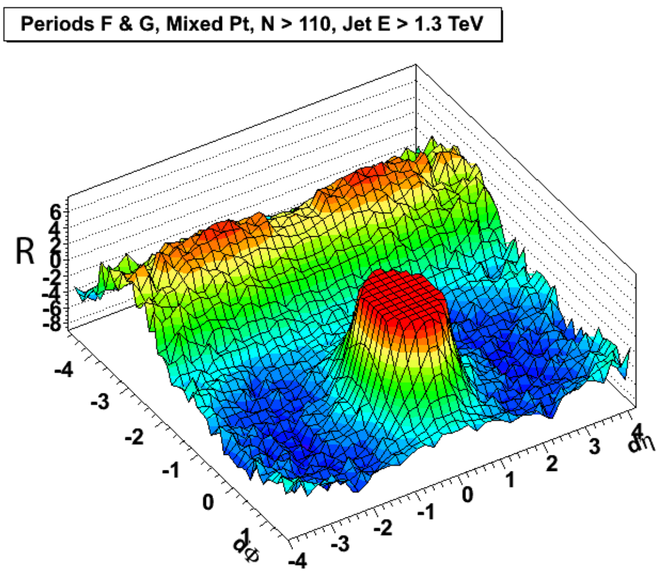

Figure 5.5: *This shows the 2-D correlation plot of the release 16 periods F & G data, with cuts of* $N > 110$ *and the sum of the total jet energy* > 1.3 *TeV, with two tracks having a* p_T *of 1 GeV/c - 3 GeV/c not allowed to be paired together.*

5.3.2 Periods H & I

To perform the analysis on the H & I data, the same cuts applied to the F & G result that seemed to show a possible ridge structure (N> 110 and total jet energy > 1.3 TeV) were implemented. This result can be viewed in Figure 5.6.

The noticeable difference between the two sets of periods persisted, with this result having no features that resembled those found in its F & G counterpart. This was still very interesting as it meant that there was a definite difference in some aspect of the data collected during the different periods, in terms of possible ridge events being recorded.

5.3.3 All Data

As the whole 2010 dataset was now available, the analysis was applied to the whole set, again with the same cuts that showed the possible ridge region in the F & G data. The result can been seen in Figure 5.7. Perhaps unsurprisingly at this stage, this result also failed to show any ridge structure, perhaps suggesting that the other periods also did not have any evidence of the ridge. This was taken with caution however, as it is known that periods F - I hold the majority of the data for the year, due to the rapid increase in luminosity. So the addition of periods A - E, was not a major increase with it only adding about 6,000 events.

At this stage, it had become a top priority to investigate which triggers were giving rise to the possible ridge structure in periods F & G.

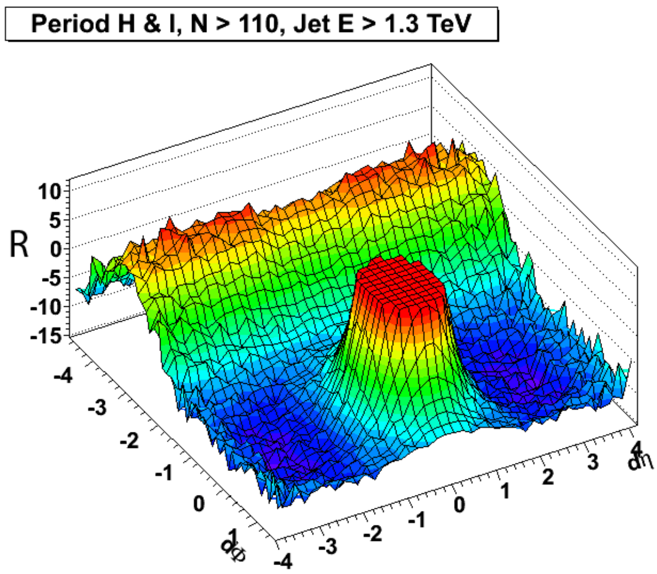

Figure 5.6: *This displays the 2-D correlation plot of the release 16 periods H & I data, with cuts of N > 110 and the sum of the total jet energy > 1.3 TeV. 25,108 events passed the cuts.*

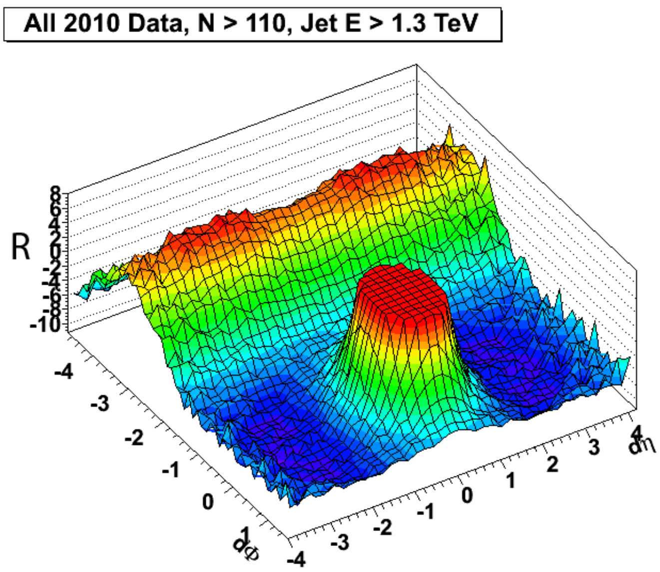

Figure 5.7: *This shows the 2-D correlation plot of the release 16 2010 data, with cuts of* $N > 110$ *and the sum of the total jet energy* > 1.3 *TeV. The cuts accepted 52,758 events.*

5.3.4 Low Multiplicity

Figure 5.8 displays results from periods F & G with the same sum of the total jet energy cut at $>$ 1.3 TeV as seen before, but now the track multiplicity had been varied. 5.8(a) had a cut of N $>$ 80 applied, 5.8(b) had N $>$ 60, and finally 5.8(c) had a N $>$ 40 cut applied. What was observed was that there existed no evidence of any structure in the region, similar to which was seen in the high multiplicity N $>$ 110. A subject that had been bothersome up to this point was the question of multiplicities connection to the colour string hypothesis as a source of the ridge. Why a high multiplicity seemed to be a necessity when searching for the ridge in a string effect environment, was a puzzling question. Yet, it seemed to be a valid requirement according to the discussed results.

Events were briefly analysed at the lower end of the multiplicity spectrum, explicitly looking at events with N $<$ 30. Figure 5.9 presents these results, which were all performed using periods F & G data. Figures 5.9(a) and 5.9(b) involve cutting on the sum of the total transverse energy of all the jets only, with requirements of $E_T > 100$ and $E_T > 200$ GeV respectively. Plots 5.9(c) and 5.9(d) on the other hand required the sum of the total energy of all the jets be $>$ 0.8 TeV and $>$ 1.2 TeV, respectively. What was observed was firstly there were no hints of any ridge structure in these low multiplicity events, this was clear. Although what was intriguing was the change in structure of the away side ridge. When the transverse energy was the subject of a cut, the away side ridge displayed a thinner width in $\Delta\phi$, but even more interestingly, when the total energy of the jets was the selection criteria the away side ridge almost vanished. The reason for this is not known, but a plausible explanation could be that it is a product of the high energy jets being extremely forward in the detector in these low multiplicity events. What was clear from these results was that they suggested the presence of the ridge was exclusive to the high multiplicity region.

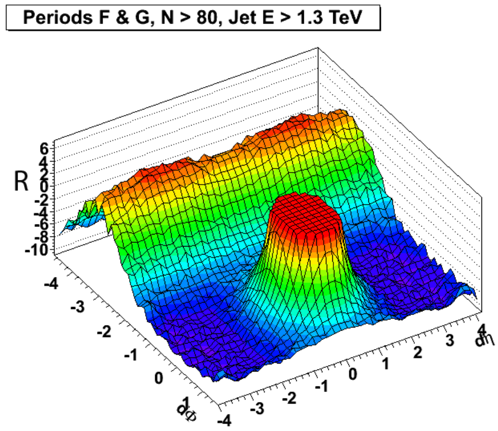

(a) N > 80

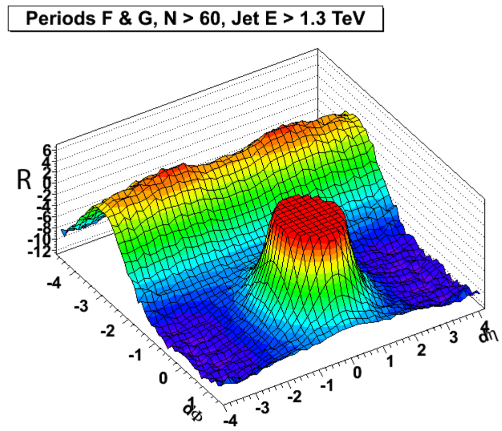

(b) N > 60

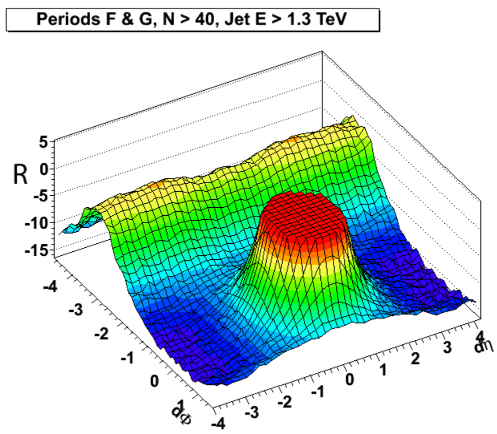

(c) N > 40

Figure 5.8: *The above shows the results of varying the track multiplicity on period F & G data, while all having the jet energy cut at > 1.3 TeV. Plots (a), (b) and (c) shows the multiplicity cut at $N > 80$ where 206,527 events passed the cuts, $N > 60$ where 715,903 events passed and finally $N > 40$ where 1.8 $\times 10^6$ passed, respectively.*

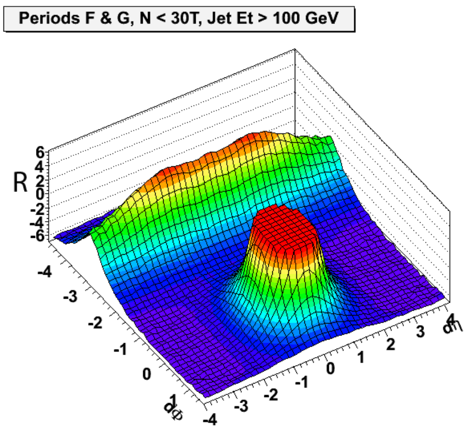

(a) Jet E_T > 100 GeV

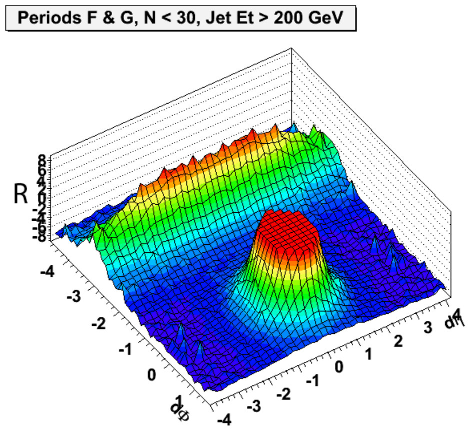

(b) Jet E_T > 200 GeV

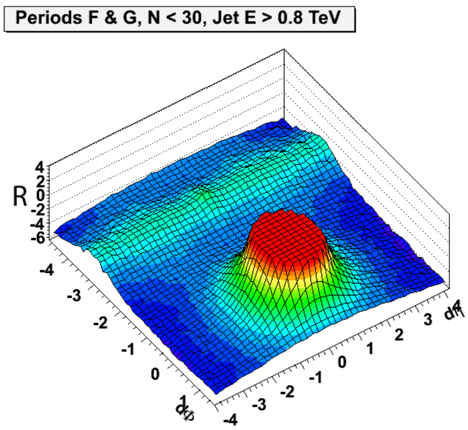

(c) Jet E > 800 GeV

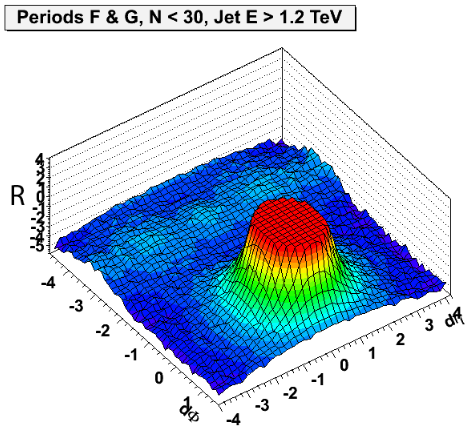

(d) Jet E > 1.2 TeV

Figure 5.9: *The above shows the results of a brief low multiplicity analysis on the period F & G data, all with* $N < 30$. *The amount of events passing the cuts were (a) 3.5* $\times 10^6$, *(b) 420, 000, (c) 2.2* $\times 10^6$ *and (d) 1.1* $\times 10^6$.

5.3.5 Trigger Analysis

By using the method outlined in Section 5.2, the data was re-analysed recording the ratio values for every trigger present in the period (achieved by simply referring to the trigger menus for each period and adding any new triggers as the lists evolved over time). Evaluating the ratio values allowed two lists to be produced, the first consisting of triggers where the first bin value was greater than the second, and the second list was simply the triggers where bin two contained the larger value. This meant that the first list represented the triggers that were potential ridge contributing candidates. This had to be taken with caution as this slightly crude method of creating the list ignores the error of the average ratio value from the profile plot. Thus, if a trigger had only one entry and was on this list, then it should be ignored. The raw ridge list from periods F & G was found to consist of the triggers as shown in Table 5.2, and although long, some can be ignored for reasons mentioned and will be revisited in Section 5.3.6.

In order to analyse the trigger results overall, a cross plot was constructed of the average ratio values of the triggers, with periods F & G on the x-axis and periods H & I on the y-axis. Figure 5.10 shows such a plot when analysing the two results previously shown from the two periods (with explicitly no trigger cuts applied). Prior to a more detailed analysis, this result immediately suggested that the individual triggers were overall quite consistent. Those contributing events to the background were perhaps slightly more so than those contributing to the ridge, but with the size of some of the errors on the outlying points, these could be ignored as being potential difference makers in terms of the ridge.

Trigger Name	Ratio Average Value	Difference from Background
EF_xe30_loose_noMu	0.00972 ± 0.00309	0.00173
EF_j30_jetNoCut	0.00893 ± 0.00077	0.00094
EF_fj30_jetNoCut	0.00868 ± 0.00174	0.0007
EF_2fj30_jetNoCut	0.00821 ± 0.00014	0.00023
EF_2fj50_jetNoCut	0.00824 ± 0.00114	0.00026
EF_te300_loose	0.0082 ± 3.8e$\times 10^{-5}$	0.00032
EF_2j30_leadingmct100_noEF	0.00878 ± 0.00183	0.0008
EF_fj50_jetNoCut	0.00815 ± 0.00012	0.00017
EF_mu4_j20_jetNoCut	0.00811 ± 0.00032	0.00013
EF_b30	0.00800 ± 0.00097	1.1×10^{-5}
EF_xe15_noMu	0.00847 ± 0.00029	0.00049
EF_2j20_jetNoCut	0.00883 ± 0.001	0.00085
EF_2j35_deta3_5	0.01048 ± 0.00121	0.0025
EF_l2j30_Trackless_HV	0.00811 ± 0.000972	0.00013
EF_2b10_3L1J10	0.00821 ± 0.00107	0.00023
EF_3b10_4L1J5	0.01179 ± 0.01179	0.00381
EF_3b10_4L1J10	0.01013 ± 0.00118	0.00214
EF_b10_IDTrkNoCut	0.00837 ± 0.00057	0.00039
EF_tau12_IDTrkNoCut	0.00969 ± 0.00165	0.00171
EF_xe20_tight_noMu	0.00801 ± 0.00013	2.5×10^{-5}
EF_tauNoCut_IdScan	0.00867 ± 0.00076	0.00068
EF_j20_jetNoEF	0.01 ± 0.00138	0.00202
EF_j30_jetNoEF	0.00826 ± 0.00070	0.00028
EF_j35_jetNoEF	0.00807 ± 0.00052	8.13×10^{-5}
EF_2fj30_jetNoEF	0.00813 ± 0.0005	0.00015
EF_fj50_jetNoEF	0.00831 ± 0.00021	0.00033
EF_j30_fj30_jetNoEF	0.00818 ± 0.00027	0.0002
EF_2j20_jetNoEF	0.01054 ± 0.00091	0.00255
EF_2j30_deta3_5_jetNoEF	0.00861 ± 0.00119	0.00063

Table 5.2: *This table shows the triggers that were picked out as being possible contributors to the ridge.*

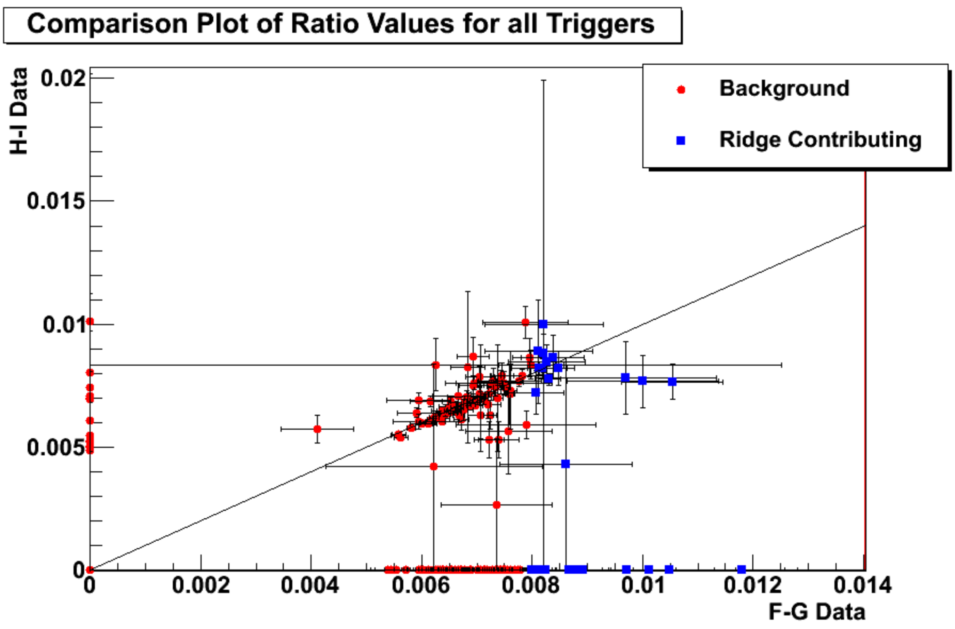

(a) Full Plot

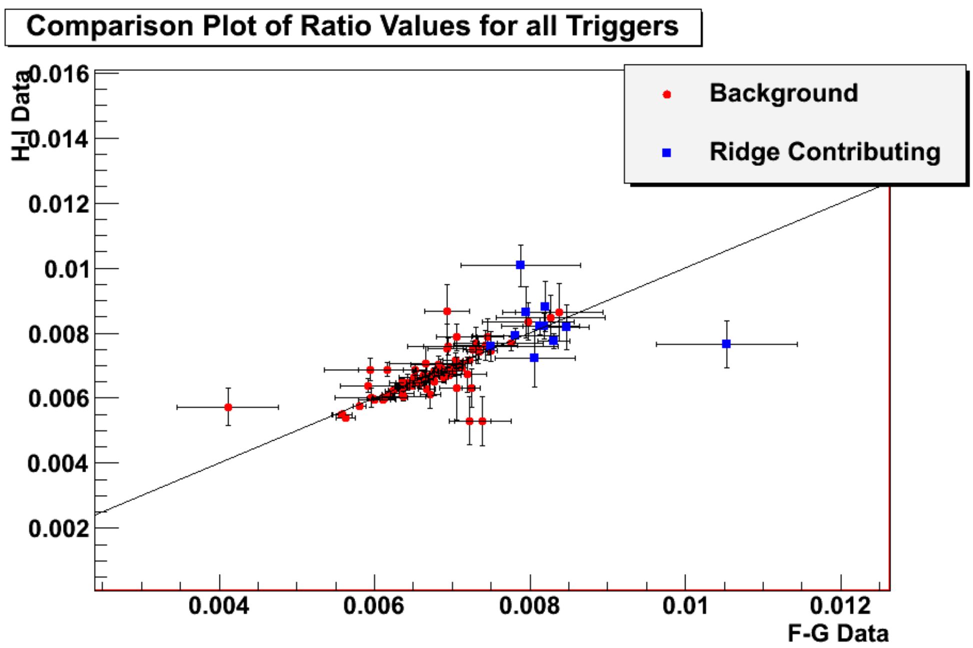

(b) Magnified View

Figure 5.10: *This presents the visual representation of comparing the average ratio values of each trigger between periods F & G and H & I. A consistent detector environment and setup would mean the points would lie on a 45° line. Plot (a) shows all the triggers involved in the analysis, with the points at either x or y equal to zero referring to those which have changed name between the periods. Plot (b) has had entries with large errors associated removed, in order to clearly see the tight correlation.*

At this point it had been observed that generally the ratio values for each individual trigger were the same, but there was still a significant observed difference in structure between the two period sets. To investigate further, another value was analysed, and this was the ratio of the number of pairs of tracks going into the ridge region divided by the total number of pairs of tracks, regardless of the trigger firing or not. This gave a numerical indication of the overall difference between the two periods. This was calculated by using the following method

$$\text{Total Ratio} = \frac{(A_{Ridge\ Triggered}\, N_{Triggered\ Ridge\ Events}) + (A_{Not\ Triggered}\, N_{Not\ Triggered\ Events})}{N_{Triggered\ Ridge\ Events} + N_{Not\ Triggered\ Events}} \ . \tag{5.2}$$

Where A is the measured ratio as given previously in Equation 5.1, and N is simply the number of entries made into the respective histogram. This ratio would be the same for every trigger so it also offered a validation of the method being carried out correctly. Table 5.3 shows the two numbers from this analysis, which were indeed the same for each trigger, but it uncovered a definite difference between the two sets of data. While at first glance appearing very similar, when taken into account that this is an average value, it was quite a significant difference. Further investigation was needed to ascertain which specific triggers were causing a discrepancy, so analyses were started where cuts were made on the trigger of the event.

Periods	Total Ratio
F & G	$0.007985 \pm 4.3 \times 10^{-6}$
H & I	$0.007409 \pm 3.6 \times 10^{-6}$

Table 5.3: *This table shows the result of calculating the total ratio for the two different period sets, taken from a trigger with a decent amount of events. This was because even though the value is the same for each trigger, the error associated can change.*

5.3.6 Trigger Cuts

Before the details presented in Table 5.2 are discussed, it was mentioned in Section 5.2 that various triggers had been added from period H onwards. This was briefly investigated, but when these triggers were removed, no difference was observed. In fact, this action's only effect was to bring an imbalance to the background contribution between the two sets of periods, thus for consistency these triggers were included throughout the following analysis, as they did not act in anyway to swamp a possible ridge.

With the information presented in Table 5.2, the triggers that had a large contribution to the ridge in the F & G data were able to be selected. The first thing that was noticed was that the trigger *EF_te300_loose*, (which meant a total energy of 300 GeV or more) had a very small error, meaning that a lot of entries were made involving this trigger. On closer inspection, this trigger contributed almost half the events that were passing the high energy cuts, thus this was a definite trigger that was contributing to the ridge. Based on this, the trigger was used as a basis to select others that would also be important. In order to select them the request was made that the error be lower than the average which was 0.00085, and then have a difference between the background average of 0.0003 or larger - similar to the te300 trigger. These selections returned six additional triggers, however only two of these were total energy or jet based; the two areas of interest. So the decision was made to ignore the remaining four as these were for different analyses and these were not desired as part of the investigation at this time. Therefore, the three main ridge contributing triggers were:

- EF_te300_loose
- EF_j30_jetNoCut
- EF_fj50_jetNoEF.

Two additional analyses were performed on the F & G data and the H & I data, where only the above three triggers were allowed to contribute to the result, and then were removed from the analysis. Both with the same requirements where a structure had been observed in the F & G data. The results are presented in Figure 5.11, and what was seen was a striking contrast. The F & G data in Figure 5.11(a) was very noisy but has a sufficient amount of statistics, 6,950 events, considering that only three triggers are being requested. H & I, shown in Figure 5.11(b), on the other hand is quite the opposite. Hardly any events made it through the cuts from these triggers with only 60 events constructing the plot, and it was believed that this was the main reason as to why there was a difference in structure between the two periods (the very few events were also the reason for the very different R scale on the H & I plot). The events that mainly contributed to a possible ridge structure in F & G simply do not seem to be triggered in the later periods.

When looking at the plots where these triggers had been removed, H & I is no different from the standard result previously seen, which was expected. However, in the F & G data some sort of structure/fluctuations persist in the ridge region, which is also unsurprising considering how many triggers contributed to this region. It was slightly odd in terms of structure however, which could be investigated further by only looking at all the triggers presented in Table 5.2, but this would be very naive to perform. The proposed theory being investigated should not have any use for a tau trigger for example, so to blindly look at these and to include other similar triggers would not be true to the investigation, without proper consideration for their theoretical value.

However, with the discussed results, the confidence in the ridge that was initially observed had dwindled significantly. Whilst the results had shown some rises in the correct places, the low statistics of the situation could not be ignored. Recalling that the plots are symmetrised, a fluctuation in the right (or wrong if preferred) place could be emphasised and incorrectly interpreted. Thus while this analysis had discovered the main cause of the difference between the two periods, the question of if a ridge was present still remained elusive.

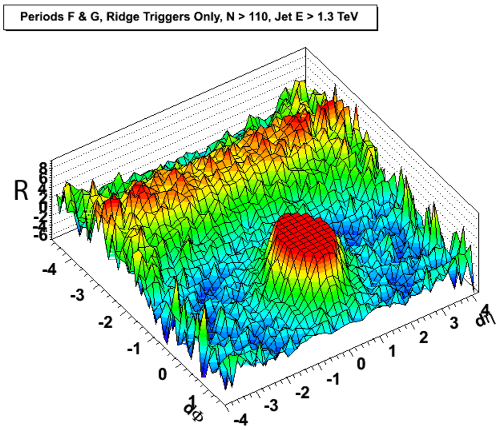

(a) Periods F & G Ridge Triggers Only

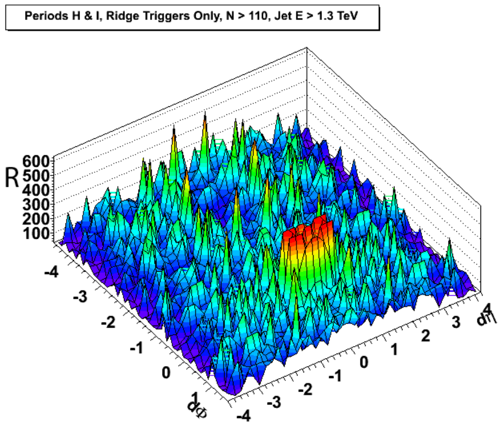

(b) Periods H & I Ridge Triggers Only

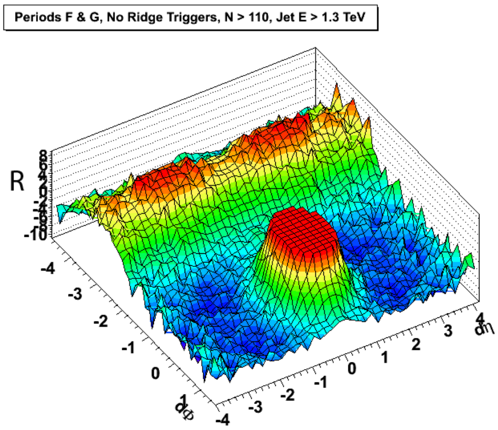

(c) Periods F & G Excluding Ridge Triggers

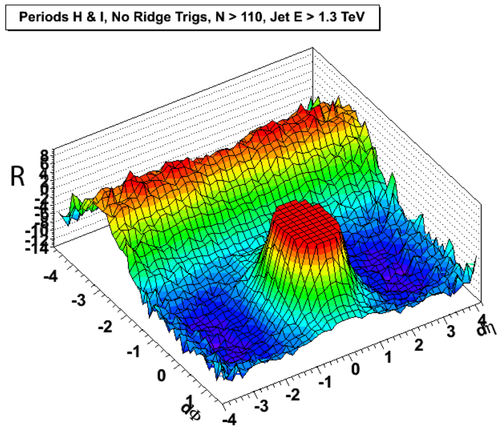

(d) Periods H & I Excluding Ridge Triggers

Figure 5.11: *Above shows the results gained when only events from the three specified triggers are analysed in (a) Periods F & G and (b) Periods H & I. Plots (c) and (d) shows the results when the three triggers are excluded from the F & G data and the H & I data respectively. Plot (a) has 6,950 events entering the plot where as (b) only has 60 events; a very significant difference. Plots (c) and (d) have 13,911 and 25,048 events respectively, which were expected as it contains simply the rest of the data.*

5.3.7 Fitting

This elusive question could be answered by an effective fitting model. The fitting was attempted to be improved by trying to better describe what was seen in the final result plot. Equation 5.3 shows the only modification that was made to the original fit model (see Equation 4.1), which was adding terms to the away side ridge to better describe its shape. This modification was only performed on the model where the ridge was described by a cosine, as this gave the best overall χ^2 value.

$$\frac{A_D}{2}[1+\cos(\phi_\Delta-\pi)](1+B_D e^{-\frac{1}{2}\left(\frac{\eta_\Delta+\beta}{\sigma_2}\right)^2}+B_D e^{-\frac{1}{2}\left(\frac{\eta_\Delta-\beta}{\sigma_2}\right)^2}) \quad . \tag{5.3}$$

With this, and by also tweaking the parameters, the fit was slightly improved but not by any meaningful significance. The result, as seen in 5.12, had a χ^2 value of 13, 977, but this still meant ≈ 6 per degree of freedom - the same as it was in release 15 fitting. Plus, the ridge parameter is still claimed to be present with a value of $2.99 \pm 2.48 \times 10^{-2}$. Unfortunately no more time was able to be spent on developing the fitting model, but this would be a main priority in any future work, in order to generate a reliable tool to test whether a ridge is present or not. Although there were hints of a ridge structure, the fitting model at its current state was not strong enough to give a definite yes or no to the structure.

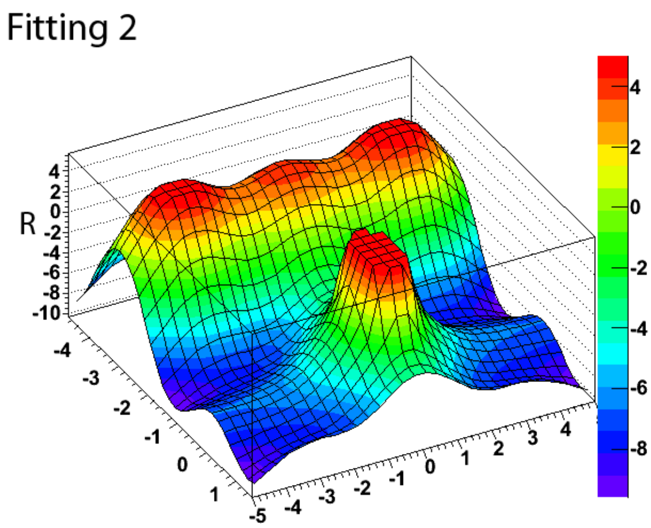

Figure 5.12: *The fitting result of the altered model.*

One other analysis was briefly run where high η di-jets were studied, with the idea of trying to select the basic events that were of interest. In short, these results added no new insight to the investigation, but the results can be viewed in Appendix B.

Chapter 6

Conclusions

The possibility of a string effect being the source of the *long-range, near-side ridge* observed in the two-particle correlation function by the CMS experiment, has been investigated using pp collisions with $\sqrt{s} = 7$ TeV recorded by the ATLAS detector. The ridge itself could be a sign of a hot, dense medium being formed in the collisions, stemming from its similarity with other ridges seen in heavy ion collisions. This ridge was observed when looking at high multiplicity events involving particles with transverse momentum, p_T, in the range of 1 GeV/c - 3 GeV/c. The study has been performed by analysing ATLAS jet stream data, mainly from the data taking periods of F-I, applying constraints with the aim of maximising a string effect as discussed in Section 2.2, while at the same time staying as true to the CMS analysis as possible.

The preliminary results of the investigation were formed using data processed by ATLAS release 15 software. An analysis with very similar cuts to that used in the CMS result showed no ridge structure, perhaps providing hints immediately that what CMS had observed was not due to a string effect, but the lack of high multiplicity statistics in the ATLAS data made it insufficient to draw a conclusion from this. However, when the analysis was tuned to become sensitive to a possible string effect, which was achieved by requesting events where the sum of the total energy of the jets was very high, while retaining the high multiplicity and track p_T range requests, a structure appeared to emerge. This was found when looking at data from periods F & G, using cuts of multiplicity, N $>$ 110, and the sum of the total energy of the jets $>$ 2.8 TeV. Yet, the result was still relatively short on statistics and a ridge caused by fluctuations could not be ruled out.

To improve the statistics of the result, data from periods H & I was added to the analysis, but surprisingly, this had the effect of diminishing the possible ridge seen in the previous periods. On closer analysis solely on the H & I data, with the same cuts as those imposed previously, simply no ridge was seen. This left two possibilities:

- The ridge seen previously was a result of statistical fluctuations.
- The assumption that high energy jets always being triggered was incorrect, and a change in trigger menus between the two sets of periods had resulted in the signal being lost.

In an attempt to eliminate the former possibility, a test was devised of performing the same analysis but this time mixing the p_T of the track pairs. Tracks were considered in the range of 0.7 GeV/c - 5 GeV/c, but a pair of two tracks both having a p_T in the range of 1 GeV/c - 3 GeV/c were not allowed to be paired together. When this was performed on the F & I data the ridge structure persisted, indicating that the structure was not due to fluctuations. This meant that the triggers of the two sets of periods needed to be investigated in order to draw further conclusions.

Fitting was also investigated using a heavy ion model, and whilst some success was achieved, the fitting attempted was not a good result, with the best fit equalling to 6 per degree of freedom. Yet in any case, the parameter used to describe the ridge in the model did return a positive and definite value with a reasonable error, once again hinting that the ridge was possibly a real signal. Heavy ion data was also briefly analysed, where a very significant ridge was observed when the analysis was applied, this acted as a nice confirmation that the method did indeed produce a ridge when expected.

When the investigation into the triggers begun, the opportunity was taken to switch the dataset to new reprocessed data produced by release 16 software. Upon re-performing the analysis from the release 16 data; its much cleaner nature meant that the previously applied cuts were very short on statistics. It was found that cuts of $N > 110$ and the sum of the total energy of the jets > 1.3 TeV resulted in a similar number of events passed as the release 15 results. In this new dataset with these cuts; the apparent ridge was a now a very faint object in the F & G data, although there was structure in the region, it was very difficult to determine whether it was a ridge or not. Applying the same mixed p_T test as before displayed no ridge, thus supporting the argument of the ridge just being caused by fluctuations. However, the difference in results between the two sets of periods persisted.

Whilst investigating the triggers between the two periods it was discovered that although they were quite consistent individually, there was a significant difference in those that could be contributing to a ridge overall. From the F & G result, the specific triggers that were contributing to the possible ridge structure were established and these were found to be total energy and forward jet triggers - exactly what the investigation involved. In fact, these triggers were responsible for $\approx 33\%$ of the 20,861 events passing the requirements in the F & G data. However, when examining the same triggers in the H & I data, only ≈ 60 events were contributed by these triggers, which was a very significant difference indeed. It was concluded that this was the main reason as to why there was a difference in appearance between the two period sets. The triggers that were contributing the most to the analysis were simply not being triggered in the H & I data.

Obviously the question still remains on the status of the actual ridge. The results from release 15 seemed to put forward a convincing case that a possible ridge was indeed present in these high energy jet events. But in light of the results from the reprocessed data the ridge has become more elusive. In the latest results, the ridge is by far not obvious and it is certainly debatable whether the structure emerging actually resembles a ridge or not, with fluctuations easily being an alternative source. Of course, if not a real signal, then the question also remains of what exactly caused what was observed in the release 15 results. There is a slight suspicion that bad jets may have contributed, as these would have been more efficiently cleaned in the release 16 data. However, how these could have provided correlations in the ridge region is unclear. There was no denying that the investigation had been starved of statistics throughout. This caused fluctuations to be of a major concern, yet a solution to this would be to simply obtain more data. Specifically, more of the high energy events which were selected by the te_300 trigger, the very same that contributed the most to possible ridge events. While fitting was briefly revisited, but sadly unable to have been advanced in a considerable way, the need for a reliable model is of high importance. This is because a reliable model would act as the tool in which a ridge could be validated as a real signal.

Definitely not observing a ridge would be an important result in itself. Throughout the analysis, a structure was observed only in high multiplicity events, with low multiplicity studies providing negative results in terms of a ridge. These such events in pp collisions are as similar as possible to the conditions seen in heavy ion collisions, where as discussed, a quark gluon plasma is believed to have been created. As acknowledged previously, this dependence on high multiplicity is a little baffling in terms of the string model, and if this is indeed the only region where the ridge is visible in, this may point towards a heavy ion like process being the source of the CMS ridge.

6.1 Future Work

The above results and conclusions naturally direct the investigation to the following areas:

- **Fitting -** As previously mentioned, the requirement for the development of the fitting model is very high. Some areas of the model need more improving over others; for example even the expression describing the ridge does not really accurately reproduce the observed feature, even from the CMS result. This would be a top priority in future work.

- **Improved Analysis -** It is not unreasonable to state that the analysis could be improved. One way to achieve this would be to observe more carefully the tracks going into the ridge region. Instead of defining a broad range in $\Delta\eta$ for the ridge, this area could be divided up with greater care as to which events are contributing where in the ridge. This could eliminate the fact that whilst one trigger displayed a high percentage of contribution, it could all be in a very small $\Delta\eta$ window.

- **More Data -** With data production successfully continuing at the LHC, more data would act to improve the statistics of the result and hopefully would remove the possibility of fluctuations being accidentally interpreted as a ridge. However, caution would have to be given to which triggers were being used in the data recording. As shown, the dominant type of triggers for this analysis are few, and can effect the results significantly if they are not running. So ideally, the te_300 trigger would be very useful to run again for a period of time.

- **Monte Carlo Data** - While untouched during the analysis because of the concentration on the real data produced by ATLAS, the comparison with simulation data would be valuable. Strings are present in most Monte Carlo generators, and so this could act as a test of the proposed theory. Even though CMS failed to see the ridge in simulation data, a specific search may bring such a feature to light.

In conclusion, the search for the long-range, near-side ridge, produced by a colour reconnecting string effect, has provided tantalising hints that a ridge might just be present in these high multiplicity, high jet energy events. However, with the investigation deprived of statistics; the inconsistency of high energy triggers; and the lack of a definite, clear ridge in the latest 2-D correlation results; there is no current evidence to support that the colour string model can produce a long-range, near-side ridge.

References

[1] CMS Collaboration. Observation of Long-Range Near-Side Angular Correlations in Proton-Proton Collisions at the LHC. 2010. 1, 2

[2] John Adams et al. Experimental and theoretical challenges in the search for the quark gluon plasma: The STAR collaboration's critical assessment of the evidence from RHIC collisions. *Nucl. Phys.*, A757:102–183, 2005. 3

[3] B. Andersson, G. Gustafson, and B. Nilsson-Almqvist. A model for low-p_T hadronic reactions with generalizations to hadron-nucleus and nucleus-nucleus collisions. *Nuclear Physics B*, 281(1-2):289 – 309, 1987. 4

[4] A Morel and G Plaut. How do clusters look in semi-inclusive cross sections? oai:cds.cern.ch:415844. *Nucl. Phys. B*, 78(CERN-TH-1865):541–551. 13 p, May 1974. 4

[5] Measurement of inclusive two-particle angular correlations in proton-proton collisions at $\sqrt{s}$ = 900 gev and 7 tev. Technical Report ATLAS-CONF-2011-055, CERN, Geneva, Apr 2011. 4, 5

[6] K. H. Ackermann et al. Star detector overview. *Nuclear Instruments and Methods in Physics Research Section A: Accelerators, Spectrometers, Detectors and Associated Equipment*, 499(2-3):624 – 632, 2003. The Relativistic Heavy Ion Collider Project: RHIC and its Detectors. 4

[7] B. I. Abelev et al. Long range rapidity correlations and jet production in high energy nuclear collisions. *Phys. Rev.*, C80:064912, 2009. 4, 7

[8] Edward Shuryak. Comments on the CMS discovery of the 'Ridge' in High Multiplicity pp collisions at LHC. 2010. 5

[9] David Griffiths. *Introduction to Elementary Particles*. Second, revised edition, 2008. 6

[10] A. Belyaev. PHYS 3002 - Nuclei and Particles Lecture Notes 2010/11. page 148, 2011. 6

[11] K. Adcox et al. Formation of dense partonic matter in relativistic nucleus nucleus collisions at RHIC: Experimental evaluation by the PHENIX collaboration. *Nucl. Phys.*, A757:184–283, 2005. 6

[12] K. Adcox et al. Hunting the Quark Gluon Plasma Assessments by Experimental Collaborations Relativistic Heavy Ion Collider (RHIC) Brookhaven National Laboratory, Upton, NY 11974-5000 Results from the First Three Years at RHIC. http://www.bnl.gov/npp/docs/Hunting 6, 7

[13] W. A. Zajc. The Fluid Nature of Quark-Gluon Plasma. *Nucl. Phys.*, A805:283–294, 2008. 6

[14] Larry McLerran. The CGC and the Glasma: Two Lectures at the Yukawa Insitute. 2010. 7

[15] K. Werner, Iu. Karpenko, and T. Pierog. The 'Ridge' in Proton-Proton Scattering at 7 TeV. 2010. 8

[16] Larry McLerran. The Ridge, the Glasma and Flow. 2008. 8

[17] Lijuan Ruan. RHIC Physics Overview. *Front. Phys. China*, 5:205–214, 2010. 8

[18] Georges Aad et al. Observation of a Centrality-Dependent Dijet Asymmetry in Lead-Lead Collisions at $\sqrt{s_{NN}}$= 2.76 TeV with the ATLAS Detector at the LHC. *Phys. Rev. Lett.*, 105:252303, 2010. 8, 26

[19] Tapan Nayak and Bikash Sinha. Search and study of Quark Gluon Plasma at the CERN-LHC. 2009. 8

[20] The ALICE Collaboration *et al.* The ALICE Experiment at the CERN Large Hadron Collider. *Journal of Instrumentation*, 2008. 8, 10

[21] The CMS Collaboration *et al.* The CMS Experiment at the CERN LHC. *Journal of Instrumentation*, 2008. 10

[22] The LHCb Collaboration *et al.* The LHCb Detector at the LHC. *Journal of Instrumentation*, 2008. 10

[23] The ATLAS Collaboration *et al.* The ATLAS Experiment at the CERN Large Hadron Collider. *Journal of Instrumentation*, 2008. 11, 12

[24] ATLAS Collaboration. ATLAS Experiment - Detector Description. *http://www.atlas.ch/detector.html*, 2011. 11

[25] Angular correlations between charged particles from proton-proton collisions at $\sqrt{s}$ = 900 gev and $\sqrt{s}$ = 7 tev measured with atlas detector. Technical Report ATLAS-CONF-2010-082, CERN, Geneva, Oct 2010. 12

[26] Matteo Cacciari, Gavin P. Salam, and Gregory Soyez. The anti- k t jet clustering algorithm. 2008(04):063, 2008. 13

[27] Beate Heinemann. Data Periods Twiki. *https://twiki.cern.ch/twiki/bin/view/AtlasProtected/DataPeriods*, 2010. 15

[28] J. Adams *et al.* Minijet deformation and charge-independent angular correlations on momentum subspace (η, ϕ) in au-au collisions at $\sqrt{s_{NN}} = 130$ gev. *Phys. Rev. C*, 73(6):064907, Jun 2006. 22

Appendices

Appendix A

Jet Cleaning

Figure A.1 defines the recommended jet cleaning cuts provided by the JetTauEtmiss group, for release 16, 2010 data, where as Figure A.2 displays the effect of the cleaning on the spectrum of the sum of the E_T of all the jets in the period F & G data.

	Loose	**Medium = Loose OR**	*****under discussion*** Tight = Medium OR**
HEC spikes	HECf>0.5 && |HECQ|>0.5 or |neg. E|>60GeV	HECf>1-|HECQ|	
EM coherent noise	EMf>0.95 &&|LArQ|>0.8 && |eta|<2.8	EMf>0.9 && |LArQ|>0.8 && |eta|<2.8	|LArQ|>0.95 or EMf>0.98 && |LArQ|>0.05
Non-collision background & Cosmics	|t|>25ns or EMf<0.05 && Chf<0.05 && |eta|<2 or EMf<0.05 && |eta|>=2 or FMax>0.99 && |eta|<2	|t|>10ns or EMf<0.05 && Chf<0.1 && |eta|<2 or EMf>0.95 && Chf<0.05 && |eta|<2	EMf<0.1 && Chf<0.2 && |eta|<2 or EMf<0.1 && |eta|>=2 or EMf>0.9 && Chf<0.02 && |eta|<2

Figure A.1: *This table defines the recommend cuts in order to remove bad jets due to detector effects.*

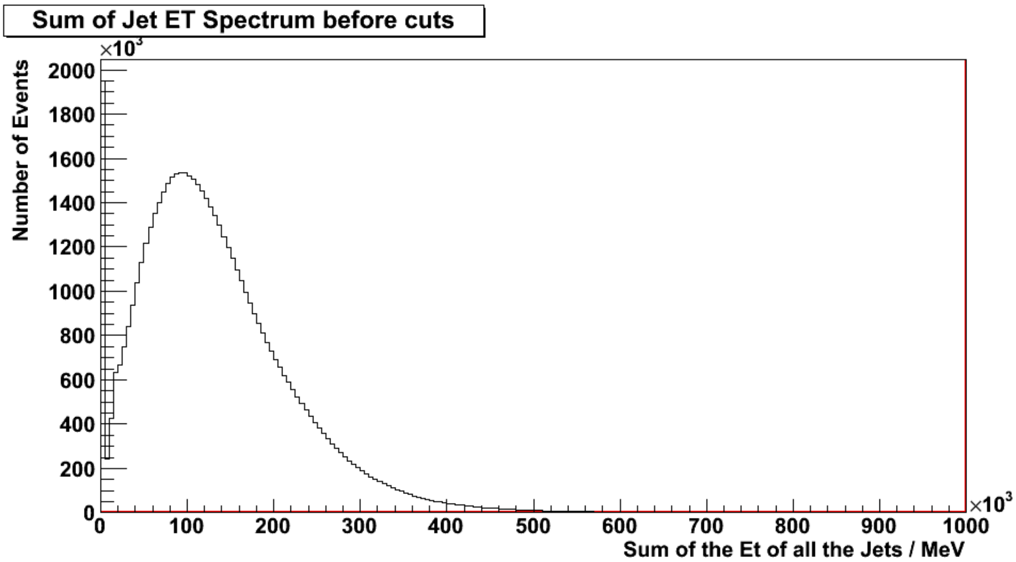

(a) Before jet cleaning

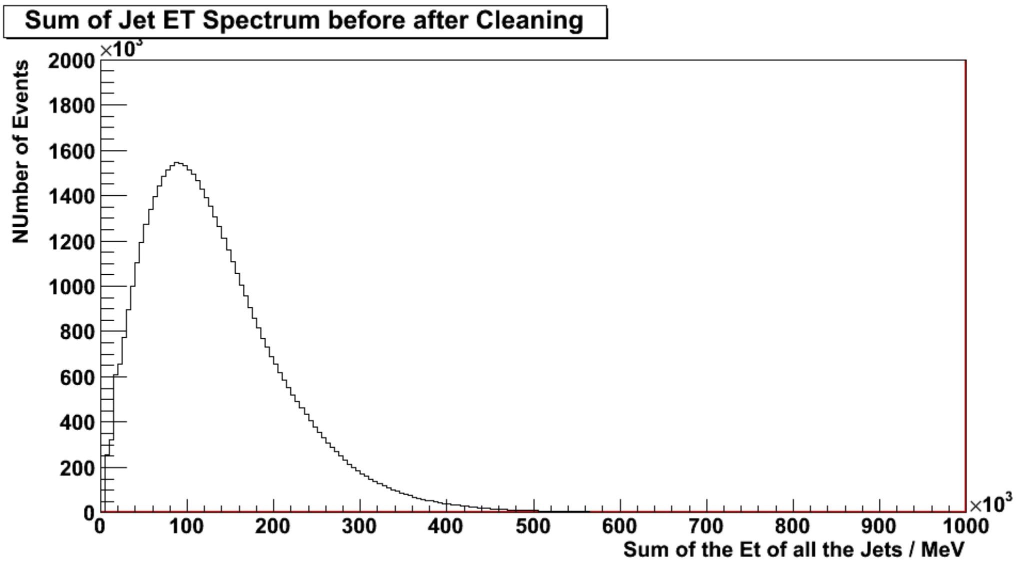

(b) After jet cleaning

Figure A.2: *This displays the spectrum of the sum of the* E_T *of all the jets in the event. (a) represents the spectrum before cleaning, and (b) after. It was noticeable how the cleaning eliminated the events with a total* E_T *of zero. Plus, a little cleaning on the main body of the spectrum.*

Appendix B

High η Di-Jet Events

The basic theory presented in Section 2.2, was a simple interaction which resulted in two jets, and to maximise a string effect, these were requested to be at a high η in the detector. Thus, we briefly analysed di-jet events where jets where only accepted if $\eta > 3$, Figure B.1 displays these results. The low multiplicity cut of N > 10 in plot B.1(a) simply displayed no evidence of any structure, which was expected with the previous low multiplicity studies. When the multiplicity cut was raised significantly to N > 80, only 924 events were accepted, which made this result invalid in terms of the ridge search. But we knew it would be quite rare to have a di-jet event with such a high multiplicity, thus this was also partly expected. While interesting to see that our basic event didn't provide any hints of a ridge structure, this investigation was not pursued any further at this time.

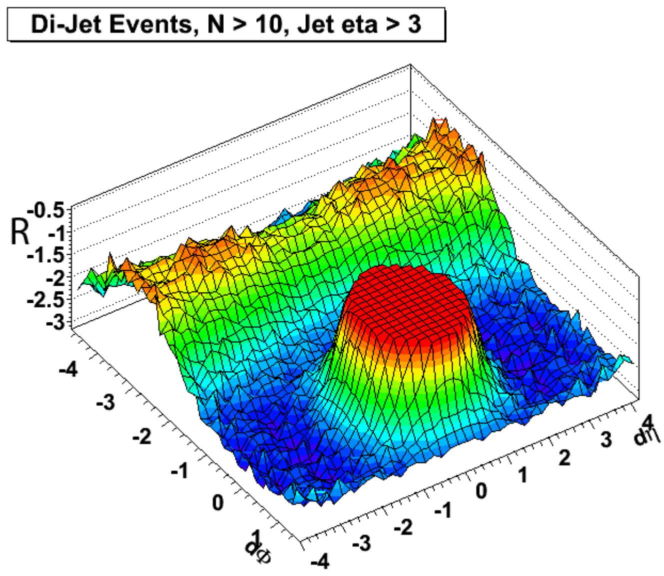

(a) N > 10

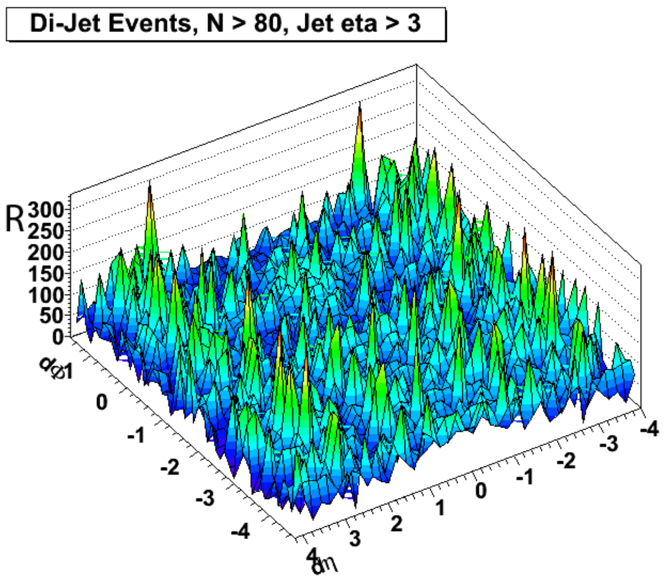

(b) N > 80

Figure B.1: *This shows the results of the brief Di-Jet analysis. While both had cuts on the accepted jets of* $\eta > 3$*, plot (a) had a track multiplicity cut of* $N > 10$ *with 4.8* $\times 10^6$ *events being accepted, while (b) had a multiplicity cut of* $N > 80$ *with only 924 events contributing.*